Computers and Chemical Engineering 135 (2020) 106760

Contents lists available at ScienceDirect

Computers and Chemical Engineering

journal homepage: www.elsevier.com/locate/compchemeng

Model compendium, data, and optimization benchmarks for sector-coupled energy systems

Susanne Sass[c], Timm Faulwasser[a,g], Dinah Elena Hollermann[d], Chrysoula Dimitra Kappatou[c], Dominique Sauer[a], Thomas Schütz[e], David Yang Shu[f], André Bardow[b,d,f], Lutz Gröll[a], Veit Hagenmeyer[a], Dirk Müller[b,e,f], Alexander Mitsos[b,c,f,*]

[a] Institute for Automation and Applied Informatics, Karlsruhe Institute of Technology, Karlsruhe 76021, Germany
[b] JARA-ENERGY, Jülich 52425, Germany
[c] RWTH Aachen University – Process Systems Engineering (AVT.SVT), Aachen 52074, Germany
[d] RWTH Aachen University – Institute of Technical Thermodynamics, Aachen 52056, Germany
[e] RWTH Aachen University – E.ON Energy Research Center, Institute for Energy Efficient Buildings and Indoor Climate, Aachen 52056, Germany
[f] Institute of Energy and Climate Research, Energy Systems Engineering (IEK-10), Forschungszentrum Jülich GmbH, Jülich 52425, Germany
[g] Institute of Energy Systems, Energy Efficiency and Energy Economics, Technische Universität Dortmund, Dortmund 44227, Germany

ARTICLE INFO

Article history:
Received 11 October 2019
Revised 24 December 2019
Accepted 24 January 2020
Available online 5 February 2020

Keywords:
Sector-coupled energy systems
Distributed energy supply system
Design optimization
Optimal control
Dynamic optimization
Benchmark problems

ABSTRACT

Decarbonization and defossilization of energy supply as well as increasing decentralization of energy generation necessitate the development of efficient strategies for design and operation of sector-coupled energy systems. Today, design and operation of process and energy systems rely on powerful numerical methods, in particular, optimization methods. The development of such methods benefits from reproducible benchmarks including transparent model equations and complete input data sets. However, to the authors' best knowledge and with respect to design and optimal control of sector-coupled energy systems, there is a lack of available benchmarks. Hence, this article provides a model compendium, exemplary realistic data sets, as well as two case studies (i.e., optimization benchmarks) for an industrial/research campus in an open-source description. The compendium includes stationary, quasi-stationary, and dynamic models for typical components as well as linearization schemes relevant for optimization of design, operation, and control of sector-coupled energy systems.

1. Introduction

Realistic mathematical models of sector-coupled energy systems are a key for developing tailored numerical optimization methods, which in turn are essential for manifold research efforts towards a successful decarbonization, defossilization, and decentralization of energy supply. Numerical optimization allows to optimally plan, design, operate, and control energy systems while accounting for the inherent volatility of renewables as well as for environmental, economic, and social aspects, see Andiappan (2017); Mitsos et al. (2018).

In process systems engineering, numerical optimization is in many cases the method of choice for control and automation problems (Engell, 2007; Engell and Harjunkoski, 2012; Kadam and Marquardt, 2007). Moreover, its importance for design optimization (Frangopoulos, 2018) and operation of energy systems is steadily increasing. The respective research efforts regarding the dynamic optimization of energy systems comprise a variety of methods and applications, spanning from the development of accurate and fast simulation methods for the control of thermal energy storage (Barz et al., 2018) via the incorporation of real-world weather forecasts (Constantinescu et al., 2011) to nonlinear model-predictive control and/or real-time optimization of power grids with storage (Adeodu et al., 2019; Braun et al., 2018; Faulwasser and Engelmann, 2019; Matke et al., 2016), and the optimization of HVAC (Heating, Ventilation, and Air Conditioning) systems for buildings (Bürger et al., 2018; Harb et al., 2015; Perez et al., 2016; Touretzky and Baldea, 2016; Zhang et al., 2014).

Design of energy systems is typically cast as Mixed-integer Nonlinear Programs (MINLPs), e.g., in Li and Barton (2015), or

* Corresponding author.
E-mail addresses: susanne.sass@rwth-aachen.de (S. Sass), timm.faulwasser@ieee.org (T. Faulwasser), dinah.hollermann@rwth-aachen.de (D.E. Hollermann), chrysoula.kappatou@rwth-aachen.de (C.D. Kappatou), dominique.sauer@kit.edu (D. Sauer), t.schuetz.1990@gmail.com (T. Schütz), david.shu@rwth-aachen.de (D.Y. Shu), andre.bardow@ltt.rwth-aachen.de (A. Bardow), lutz.groell@kit.edu (L. Gröll), veit.hagenmeyer@kit.edu (V. Hagenmeyer), dmueller@eonerc.rwth-aachen.de (D. Müller), amitsos@alum.mit.edu (A. Mitsos).

https://doi.org/10.1016/j.compchemeng.2020.106760

Mixed-integer Linear Programs (MILPs), e.g., in Lara et al. (2018); Mancarella (2014); Zhang et al. (2019). Besides, dynamic optimization problems comprising operational optimization and optimal control are typically solved by direct methods based on discretization, yielding MINLPs, NLPs (Nonlinear Programs), or MILPs, see Biegler and Grossmann (2004); Grossmann and Biegler (2004). Optimization problems arising in context of sector-coupled energy systems are challenging for a number of reasons: multiple time scales, large number of equations, uncertainties, potentially conflicting multiple objectives, or the hard-to-quantify effect of underlying modeling assumptions. Hence, there are widespread and ongoing research efforts on modeling and numerical optimization for such systems, see, e.g., Barton (2009); Faulwasser et al. (2018); Majewski et al. (2017); Mühlpfordt et al. (2018); Roald et al. (2017).

The development of any numerical method benefits from well-defined, transparent, and realistic benchmark problems. In numerical optimization, benchmark libraries are therefore widely established, including MINLPLib (Bussieck et al., 2003), PrincetonLib (Vanderbei et al., 2004), COCONUT benchmark (Shcherbina et al., 2002), MINTOC benchmark (Sager, 2012), and MIPLIB (Koch et al., 2017). Benchmark problems are also common in Process Systems Engineering such as the Williams-Otto reactor (Williams and Otto, 1960), which, up to this day, is frequently used to compare methods for real-time optimization of process systems (Srinivasan and Bonvin, 2019). Another well-known benchmark problem is the Tennessee Eastman process proposed by Downs and Vogel (1993). It is still in use for a wide range of research purposes, e.g., for demonstrating the efficiency of a newly developed plant-wide control scheme (Luppi et al., 2018). Recently, similar efforts have been made for energy systems. This includes

- software frameworks for modeling and optimization of sector-coupled energy supply systems available online, compare for example Augenstein et al. (2005), Ringkjøb et al. (2018), Schütz et al. (2017), and the Temoa framework with the widely accepted linear and quasi-stationary benchmark model Utopia (Howells et al., 2011; Hunter et al., 2013);
- a lately increasing number of open source data-bases providing country-scale data like the Open Energy Modeling Initiative (Open Energy Modelling Initiative, 2019) or specifications of complete power plants like the JRC Open Power Plants Database (Hidalgo Gonzalez et al., 2019);
- benchmarks for specific energy systems like electricity grids (IEEE, 2018; Hörsch et al., 2018; University of Washington, 2018) or energy supply systems for supermarkets as used, e.g., in Beykal et al. (2018); and
- specifically focused model collections, e.g., for ship energy systems (Sakalis et al., 2019) or for economic design of combined cooling, heating, and power (CCHP) systems (Rech, 2019).

However, there are also certain shortcomings and gaps in the benchmarks available in the literature.

- The existing software frameworks usually lack transparency. Typically, there is no easily accessible documentation of model equations and corresponding example data.
- Existing data-sets do not account for the scale of an industrial/research campus or specifications of individual components like boilers.
- Specific benchmarks and model collections lack flexibility. If the focus is on a particular sector-coupled energy system, different objectives, or the combination of quasi-stationary and dynamic operation of different components, the adaptation of the proposed setting is usually time consuming or even effectively impossible due to a lack of documentation.

To the best of the authors' knowledge, there is currently no widely accepted benchmark for the optimization of design, operation, and control of energy systems supplying industrial/research campuses. Moreover, models and especially input data for such energy systems are scattered over numerous publications, specification sheets, websites, etc. and are often subject to data protection regulations.

Thus, we compile a model compendium for typical components of an energy supply system coupling cooling, heating, and electricity for industrial/research campuses. The considered setting is inspired by the real-world supply systems of the Campus North of the Karlsruhe Institute of Technology and the Forschungszentrum Jülich.[1] We provide a complete data set for weather, energy prices, cooling, heating, and electricity demands as well as parameter values for the system components. On the demand side, we include building models validated with real-world measurements. The application setting considered is the optimal design and operation of industrial/research campuses. In principle the scope of the models could be extended to include industrial processes and large-scale networks; however, this is outside the scope of the manuscript. Finally, we propose two optimization case studies as open-source benchmark problems: (1) a bi-objective design optimization of a generic energy system and (2) the operational optimization of a dynamic model for a sector-coupled energy system with fixed design.

We address requirements of different application contexts, namely the optimization of design, operation, and control of energy systems. Hence, we include stationary, quasi-stationary, and dynamic model equations of the most frequently considered components. We do not attempt an extensive review on modeling strategies or data ranges. Rather we present one common model formulation for each component. These models are based on already available publications and specification sheets. In fact, the components are modeled based on energy flow rates, which have to satisfy energy balance equations and input-output-relations given by efficiency or COP (coefficient of performance) curves, i.e., they are first-principles models. For the sake of self-containment, we recall a linearization scheme (Voll et al., 2013) and an approach for considering a minimum load fraction within the purely continuous and smooth dynamic optimization model of our second benchmark case study based on standard techniques. To foster accessibility of the compendium, we propose a consistent notation.

The remainder of this article is structured as follows: In Section 2, we present the virtual campus including all components of an energy supply system, which are considered in this article. Based on this *generic energy system*, we emphasize how the consistent notation and modeling of our corresponding model compendium allows for identifying synergies and structural differences of the various fields of applications. Section 3 contains description and results of the two benchmark case studies. Finally, conclusions are drawn in Section 4. The Appendix starts with the introduction of the notation in Appendix A. Afterwards, the model compendium including example parameter values forms Appendix B. In Appendix C and Appendix D, the linearization scheme and a smooth extension of the dynamic equations regarding a minimum load fraction, respectively, are given. The git repository available at https://git.es2050.org/heci/energy-benchmark contains input and output data as well as the models and optimization formulations in GAMS (McCarl and Rosenthal, 2016), Modelica (Mattsson and Elmqvist, 1997), and Pyomo http://www.pyomo.org/.

2. Generic energy system for a campus

Fig. 1 shows the generic structure of a sector-coupled energy supply system for a campus of variable size considered in this arti-

[1] This article is a contribution to the open source and benchmark project HECI – *Helmholtz Energy Computing Initiative* (HECI, 2019).

cle. The eventual choice of components, number of respective units as well as coupling points between the gas, electricity, heating, and cooling grid is subject to the specifically chosen application. Both economic and environmental criteria can be chosen for evaluating design and operation of the generic energy system.

To cover the specific needs of the optimization of design, operation, and control of energy supply systems, consistent quasi-stationary and dynamic models as well as linear and nonlinear models are provided. The quasi-stationary models can be obtained by setting all temporal derivatives to zero in the dynamic models. Similarly, the linear models converge to the nonlinear models in the limit of zero distance between two adjacent supporting points. As a result, the gathered component models form a unified framework, which allows to investigate the impact of linearizations and the assumption of quasi-stationary behavior for the optimization of energy supply systems without distortions caused by different modeling premises. Note that we present only models based on energy flow rates. Moreover, we provide dynamic extensions for models with thermal inertia on a scale of minutes. In contrast, models referring to electricity are assumed to be (quasi-)stationary, since the dynamics of electrical processes is usually on a scale of seconds.

The model compendium aims to emphasize synergies and structural differences between optimization applications in energy supply systems. For instance, the incorporation of battery models intrinsically introduces nonsmoothness/nonconvexity in any optimization problem, cf. discussion in Appendix B.5.2. Moreover, some degrees of freedom of a model depend on the type of component rather than the field of optimization: the input power/heat transfer rate is strictly determined by the output for conversion components, only bounded by the technical possible output for generation components and loosely coupled to the output via storage level and capacity for storage components. However, other degrees of freedom depend on the field of application and increase the complexity of the optimization problem significantly, even if the same model equations are used. E.g., the linearization scheme of the efficiency or COP in Appendix C.1 is sufficient for operational optimization problems with a-priori known capacities, while it needs to be combined with Glover's reformulation (Glover, 1975) in design optimization problems where capacities are degrees of freedom. Besides, the choice between algebraic and dynamic optimization can influence the mathematical properties of the same physical variable. As an example, the roles of input and output heat transfer rate of a boiler are interchangeable for the optimizer within a quasi-stationary, algebraic problem, see Eq. (B.4a), while their hierarchy is fixed in the dynamic model, see Eq. (B.5).

3. Optimization benchmarks

As a proof-of-concept as well as to show the wide range of applications of the provided model compendium, we propose two case studies as optimization benchmarks: (1) a bi-objective design optimization accounting for economic and environmental criteria based on all components of the generic energy system depicted in Fig. 1, and (2) a dynamic operational optimization of a sector-coupled energy supply system with fixed, optimal design. Both case studies consider the demand of six office buildings of type "OB", two smaller office buildings of type "OBM", and two experimental facilities "EF", each with one thermal zone, see Appendix B.2.2 for details. More specifically, Appendix B.2.1 describes the parameter identification of the thermal models for the office building "OB 1" as well as the experimental facility "EF 1" based on measured temperature data. Figs. 2 and 3 show an excerpt of the simulated temperature and heating/cooling input Q_z^{dem} compared to the real measurement data for buildings "OB 1" and "EF 1". The Coefficients of Variation of Root Mean Square Error CV(RMSE) (acc. to Coakley et al. (2014)) of the indoor temperature are 1.2% for "EF1" (for hourly data between 13 Jan and 11 Sep 2018) and 0.3% for "OB1" (for hourly data between 1 Jun and 31 Dec 2018).

Example values for general parameters and inputs as well as all model equations can be found in Appendix B. Parameter values which differ for the two case studies are given in the following. This includes, e.g., bounds on capacities which are required for the design optimization and fixed to the nominal value for the optimization of the operation.

We scale the values of system variables within the optimization models to a range of approximately 0 to 1 to avoid numerical problems.

3.1. Design optimization

Design optimization has to cope with large-scale optimization problems, in particular, due to the incorporation of combinatorial decisions and operational optimization (Frangopoulos et al., 2002). Goderbauer et al. (2019) have even shown that the design problem of (distributed) energy supply systems is NP-hard. In this case study, we regard both minimum costs and minimum global warming impact, which further increases the complexity of the design optimization problem. Thus, the models are linearized as described in Appendix C, allowing for continuous sizing of all components. Additionally, the time-varying input parameters are aggregated using the k-medoids method proposed by Bahl et al. (2018b). Thereby, we employ 4 typical periods and 4 segments per typical period with additional peak values for demands. The resulting sorted aggregated time-varying demands and prices are shown in Fig. 4 and are available at https://git.es2050.org/heci/energy-benchmark in directory "3_1_Design_Optimization" in file "AggregatedTimeSeries.csv". Despite the clear deviations between the aggregated and the original full time-series, aggregating time-series have been shown to lead to near-optimal solutions in studies (Bahl et al., 2018a; Baumgärtner et al., 2019).

All components of the generic energy system depicted in Fig. 1 are considered for the supply of a campus comprising ten buildings. Only wind turbines are excluded as the installation is often prohibited due to construction limits as, e.g., minimal distances to neighboring residential buildings. The values of Voll (2013) are used for parameters regarding boilers $\mathcal{BOI}$, combined heat and power engines $\mathcal{CHP}$, absorption chillers $\mathcal{AC}$, and compression chillers $\mathcal{CC}$, while the parameter values of Baumgärtner et al. (2019) are taken for the photovoltaic units $\mathcal{PV}$, heat pumps $\mathcal{HP}$, batteries $\mathcal{BAT}$, and thermal energy storage units $\mathcal{TES}$, see Tables 1 and 2. Note that the corresponding references had demonstrated the linearization to be an adequate representation of the nonlinear models. Example values for linearized part-load behavior and linearized investment costs are given in Tables C.1 and C.2, respectively. Please note that cyclic conditions apply for the operation of the thermal storage units as well as the battery in each typical period. Further, charge and discharge of all storage units are suppressed in the time steps representing the additional peak demand values. We assume a constant global warming impact for the electricity mix of the grid $gwi^{el} = 561\,\mathrm{g_{CO2-eq.}/kWh}$. As an alternative, a time dependent global warming impact based on Baumgärtner et al. (2019) is provided for the considered time-series as well, see "AggregatedTimeSeries.csv" at https://git.es2050.org/heci/energy-benchmark in "3_1_Design_Optimization". When electricity is fed into the grid, we assume a credit for the global warming impact **GWI** (B.1.2) following the idea of the avoided burden (Baumann and Tillman, 2014). Moreover, we employ $\mathbf{gwi}^{\text{fuel}} = 244\,\mathrm{g_{CO_2-eq.}/kWh}$ for the specific global warming impact of purchased gas as well as time horizon $\tau^{\text{h}} = 4\,\mathrm{a}$ and interest rate $\boldsymbol{\gamma}_5 = 8\,\%$ for the calculation of the present value factor **PVF** (Majewski et al., 2017). The interest

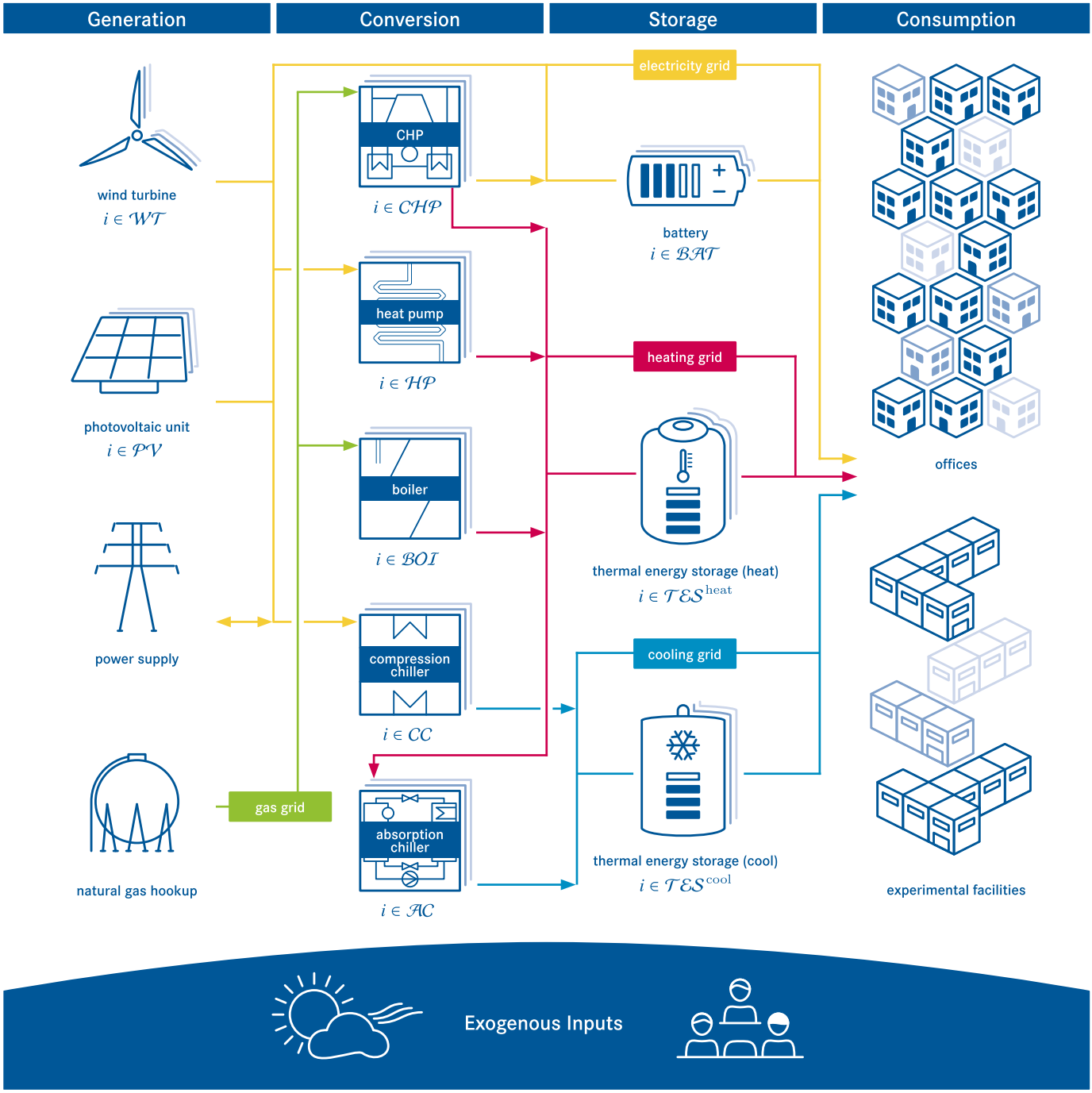

Fig. 1. Generic energy system with a free number of component units for the supply of a virtual real-world campus of office buildings and experimental facilities

Table 1
Component specifications

Comp.	Min. capacity $\mathbf{Q}_i^{\min}$ [kW]	Max. capacity $\mathbf{Q}_i^{\max}$ [kW]	Min. load fraction $\boldsymbol{\lambda}_{i,1}^{\text{out}}$ [−]	maintenance factor $\boldsymbol{\gamma}_{4,i}$ [a^{-1}]
$\mathcal{BOI}$	100	2000	0.2	0.015
$\mathcal{CHP}_1$	100	1400	0.5	0.1
$\mathcal{CHP}_2$	1400	2300	0.5	0.1
$\mathcal{CHP}_3$	2300	3200	0.5	0.1
$\mathcal{AC}$	100	2000	0.2	0.01
$\mathcal{CC}$	400	10000	0.2	0.04
$\mathcal{PV}$	5	550	0.0	0.01
$\mathcal{HP}$	5	200	0.2	0.01

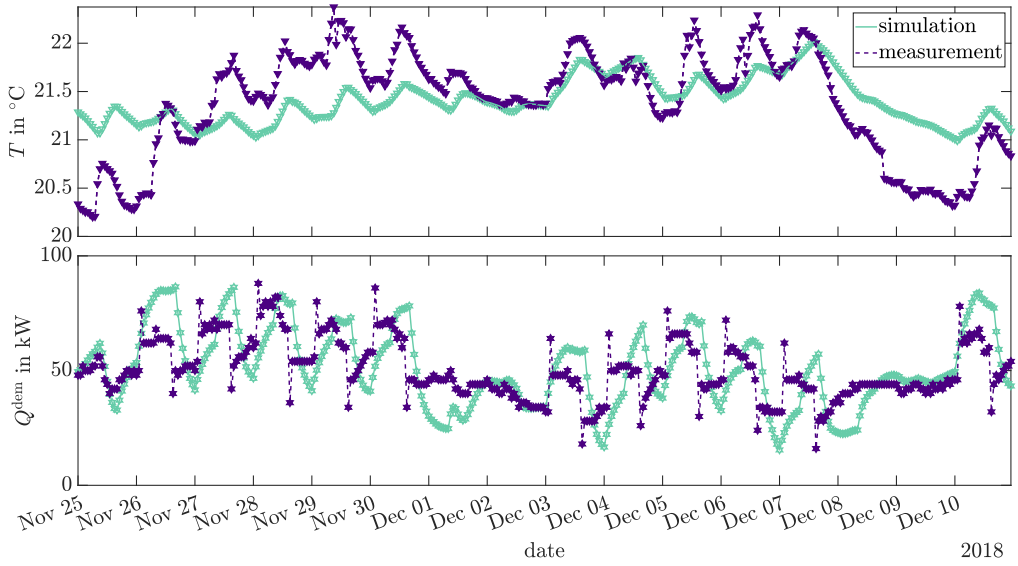

Fig. 2. Comparison of simulation and measurements for the original office building "OB 1"

Table 2
Storage component specifications

Comp.	Min. capacity $\boldsymbol{E}_i^{\min}$ [kWh]	Max. capacity $\boldsymbol{E}_i^{\max}$ [kWh]	maintenance factor $\boldsymbol{\gamma}_{4,i}$ [a^{-1}]
$\mathcal{BAT}$	0	2000	0.025
$\mathcal{TES}^{\text{cool}}$	0	25000	0.01
$\mathcal{TES}^{\text{heat}}$	0	115000	0.01

rate in application cases strongly varies; other authors employ 5 % for example (Schütz et al., 2017).

To solve the design optimization problem, we apply the automated super-structure-generation approach from Voll et al. (2013). This approach successively performs superstructure optimization until the objective function value does not further improve. In each optimization, the superstructure of the energy supply system is enlarged by one unit for each component type. Although we consider three sizes of combined heat and power engines $\mathcal{CHP}$, see Table 1, we only allow one additional CHP unit rather than one for each size when increasing the superstructure by one unit. To decrease the computational effort, we aggregate the roof area of the office buildings and of the experimental facilities, respectively, and we allow at most one photovoltaic unit and one storage component for each building type. Note that the values for the linearized investment costs are not changed despite the aggregation, since there is no significant economy of scale for photovoltaic components.

The design optimization approach is implemented in GAMS 24.7.3 (McCarl and Rosenthal, 2016). We choose GAMS as it is one of the standard modeling environments. To solve the problem, CPLEX 12.6.3.0 (IBM Corporation, 2015) is used employing an optimality gap of 0.5 %. A GAMS file containing the problem statement after automated super-structure generation and using the single objective of total annualized costs, namely "Model.lst", can be found at https://git.es2050.org/heci/energy-benchmark in "3_1_Design_Optimization". Therein, we also provide a corresponding pyomo file generated automatically via the GAMS convert function, along with the variable mapping. Pyomo has the advantage that it is open source.

We perform a bi-criteria optimization, minimizing the total annualized costs **TAC** and the global warming impact **GWI** employing the augmented ε-constraint method (Mavrotas, 2009). The resulting trade-off in the Pareto front as well as the corresponding Pareto-efficient designs are shown in Fig. 5.

The global warming impact **GWI** decreases for designs with a tri-generation system in place of separately operating boilers $\mathcal{BOI}$ and compression chillers $\mathcal{CC}$ with additional purchase of electricity from the grid. Low-**GWI** energy systems employ a higher number of CHP engines in combination with the installation of absorption chillers $\mathcal{AC}$, which allows for simultaneous heating and cooling supply while providing electricity for on-site demands or the grid. As a result, the system is even able to reach a negative global warming impact **GWI**, as the avoided burden by feeding in electricity (Appendix B.1.2) is higher than the global warming impact induced by the consumption of fuel on-site.

The increasing investment in a higher number of smaller conversion units and larger storage units enables a more ecological operation by utilizing highly-efficient operational points and load shifting, compare Fig. 5(b). Moreover, larger photovoltaic units are installed for a more climate-friendly energy supply. The maximum PV area is reached at the third point on the Pareto front with decreasing global warming impact **GWI**.

Herein, we do not consider the selection of a final design by the decision maker. This selection can be done with a wide range of decision supporting tools, see, e.g., Jing et al. (2019). For the synthesis of distributed energy supply systems and other two-stage optimization problems, for instance, the *flex-hand approach* automatically selects a highly flexible design in operation such that the final design performs well regarding all considered criteria (Hollermann et al., 2019).

3.2. Operational optimization

The second case study pertains to the offline optimal control of nominal operation based on realistic simulation data and parameter values as well as the dynamic models given in Appendix B with the extension discussed in Appendix D. The energy supply system considered is given by the cost-optimal solution of the design optimization problem discussed in Section 3.1. We particularly focus on the parallels between thermal energy storage (TES) and the thermal inertia in buildings.

The feasibility of the design for an energy system with either explicit or implicit storage is guaranteed by excluding TES units in the design optimization. Instead, the size of the TES unit is adapted to heat transfer capacity $\boldsymbol{Q}^{\max} = 100$kW of Building "OB

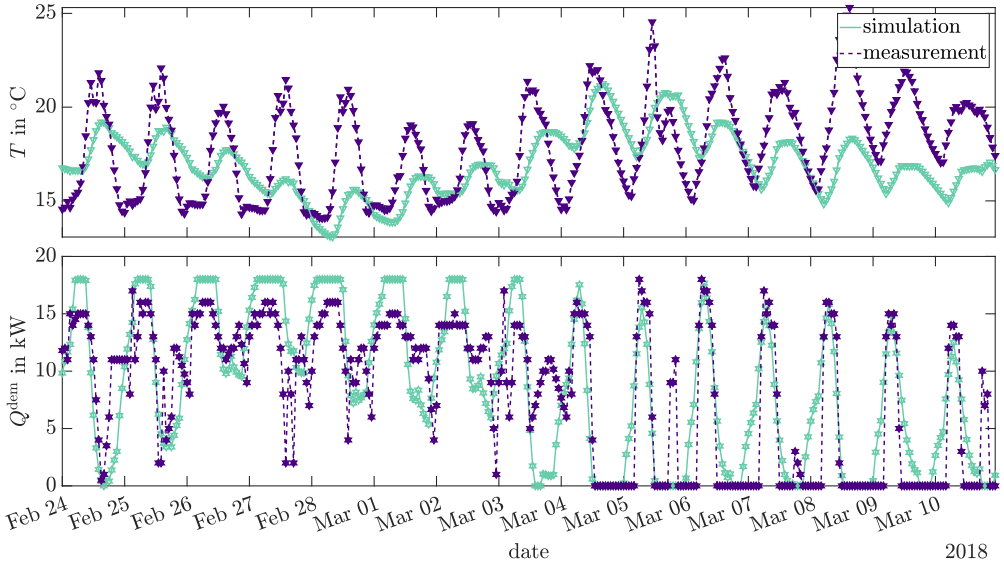

Fig. 3. Comparison of simulation and measurements for the original experimental facility "EF 1"

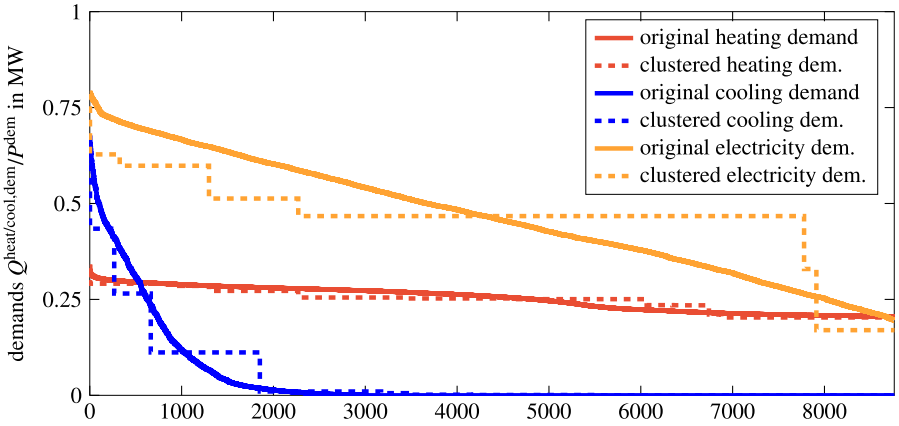

(a) Demands

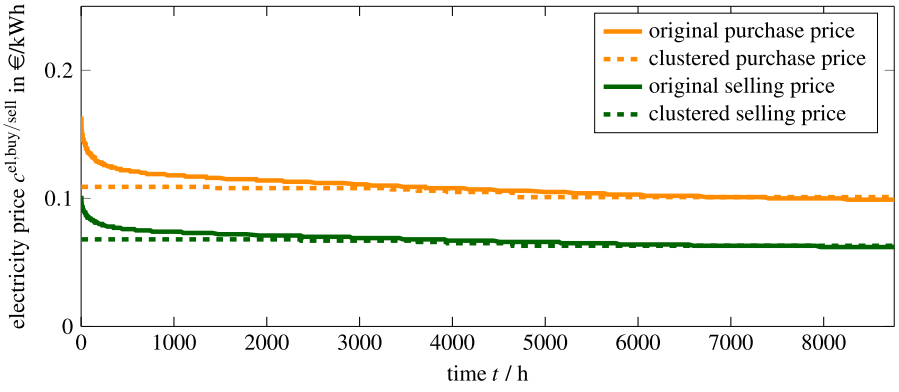

(b) Prices

Fig. 4. Sorted full as well as sorted time-aggregated energy demands and prices used in the design optimization

1", cf. Table B.3, by choosing nominal capacity $\boldsymbol{E}_i^{\text{nom}} = 1\text{h} \cdot \boldsymbol{Q}^{\text{max}} = 100\text{kWh}$, cf. Appendix B.5.1. The optimal design comprises one boiler unit with nominal capacity $\boldsymbol{Q}_i^{\text{nom}} = 530\text{kW}$, $i \in \mathcal{BOI}$ and minimum load fraction $\boldsymbol{\lambda}_i^{\text{min}} = 0.2$, $i \in \mathcal{BOI}$, one CHP unit with nominal capacity $\boldsymbol{Q}_i^{\text{nom}} = 470\text{kW}$, $i \in \mathcal{CHP}$ and minimum load fraction $\boldsymbol{\lambda}_i^{\text{min}} = 0.5$, $i \in \mathcal{CHP}$, as well as PV units covering the maximum possible surface area of the solar panels on the buildings, cf. B.4.1. For the energy conversion components, time constants $\boldsymbol{\tau}_i = 0.1\text{h}$, $i \in \mathcal{BOI} \cup \mathcal{CHP}$ are chosen due to their fast response in reality.

We use weather data of Stuttgart in the winter week November 26, 2018 to December 02, 2018 (DWD Climate Data Center (CDC), 2018) and the price data of a similar week during the year, namely

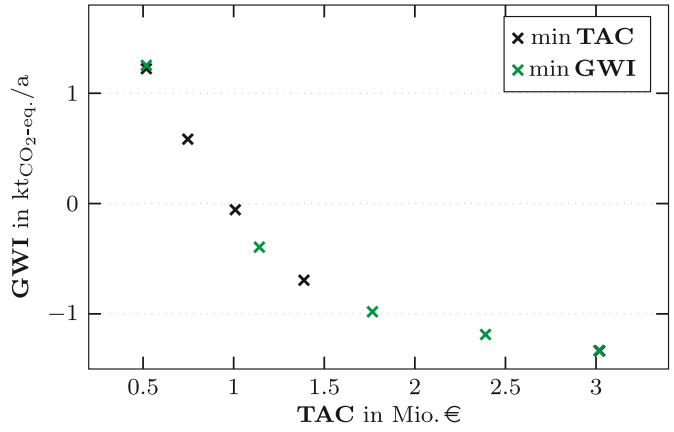

(a) Pareto front computed employing the augmented ε-constraint method (Mavrotas, 2009), i. e., by minimizing the total annualized costs **TAC** while limiting the global warming impact **GWI** (×) and vice versa (×)

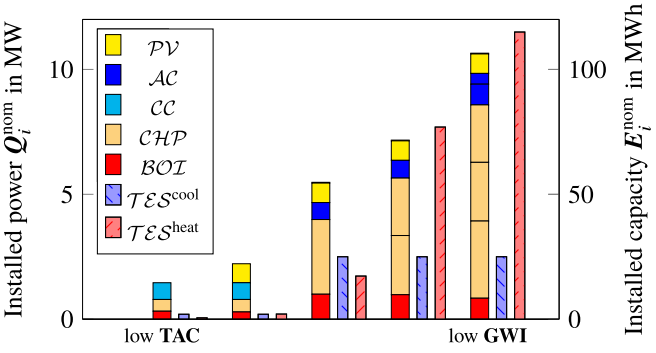

(b) Designs on Pareto front for the green crosses (×) of Fig. 5(a) from left to right with decreasing global warming impact **GWI**; left axis relates to conversion as well as generation components and right axis to storage components

Fig. 5. Designs of Pareto-efficient solutions based on possibly installed components shown in Fig. 1

time points 7896h - 8063h taken from Bahl et al. (2018b), see Fig. 6.

The controls are the heat transfer input of the boiler and the CHP unit, the power provided by the PV components clustered in one unit for all (modified) office buildings and one for both experimental facilities, as well as the purchased electricity at any considered time point. The initial values of the load fractions of boiler and CHP are optimized. The TES is set to be half-full at the beginning to allow for both charging and discharging. The heat transfer rate exchanged with the TES is the difference between the given demand and the heat transfer rate provided by the boiler and the CHP unit. We minimize the total costs subject to the model constraints reported in Appendix B. Note that violations of path constraints may occur between discretization points, compare Fu et al. (2015). Besides, we do not impose periodic boundary conditions to not further restrict the optimizer. Since weather is not week-periodic, periodic operation is not expected to be optimal. Other researchers, e.g., (Ghobeity and Mitsos, 2012) have imposed periodic boundary conditions to avoid discharging the storage. Our model compendium enables variations of the benchmark to account for such boundary conditions. Note however that periodic boundary conditions and oscillating systems bring substantial challenges (Wilkins et al., 2009).

For the dynamic optimization of the operation, the dynamic optimizer DyOS (Caspari et al., 2019; DyOS, 2019) calling local nonlinear optimizer SNOPT (Gill et al., 2005) and integrator IDAS (Serban et al., 2018) is employed. We use feasibility tolerance of 0.01 and optimality tolerance of 0.001. We write the model in Modelica. The motivation is that it is open source and supported by a variety of commercial and open-source simulation and optimization tools, including our in-house solver DyOS. In nonconvex dynamic optimization problems, a good initial guess is typically required for convergence of the optimizer. While in principle deterministic global methods exist since more than a decade (Singer and Barton, 2006), these are far from being applicable to such systems. An alternative are heuristic local methods such as multistart, which has been applied to energy systems, e.g., (Ghobeity and Mitsos, 2012). However, a challenge is that many runs fail to converge. Herein, we find the initial point based on ad-hoc adaptations of intermediate optimization results. Flat Modelica files containing the dynamic optimization problem as well as the dynamic simulation model for building "OB 1" are given by "OptModel.mo" and "OB1SimModel.mo", respectively, at https://git.es2050.org/heci/energy-benchmark in directory "3_2_Optimal_Control".

The CHP over-fulfills the electricity demand when the gas price is low and the gas demand is high compared to the electricity demand, cf. Fig. 7(b). Thus, no purchase of electricity is required and only the volatility of the sale price of electricity can affect the optimal solution. In this way, the TES enables a higher CHP load in periods with higher sale prices for electricity. For instance Fig. 7(a) shows the CHP extended full-load period within interval [18h, 24h] and the load fraction peak within interval [150h, 168h]. In contrast to that, the boiler is only used during the high demand periods of the workdays, i.e., from 0h to approximately 120h. To satisfy the remaining heat demand, the boiler is run at about 30 % to 40 % load, see Fig. 7c. Note that the operation with this low load fraction is already highly efficient, cf. Fig. D.1. At the weekend, the bi-

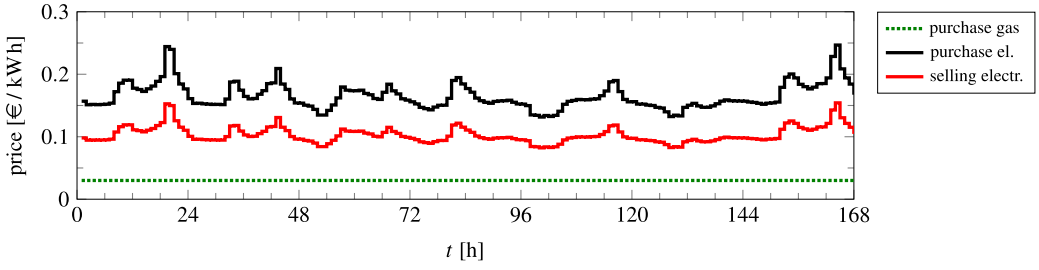

Fig. 6. Electricity and gas costs taken from Bahl et al. (2018b)

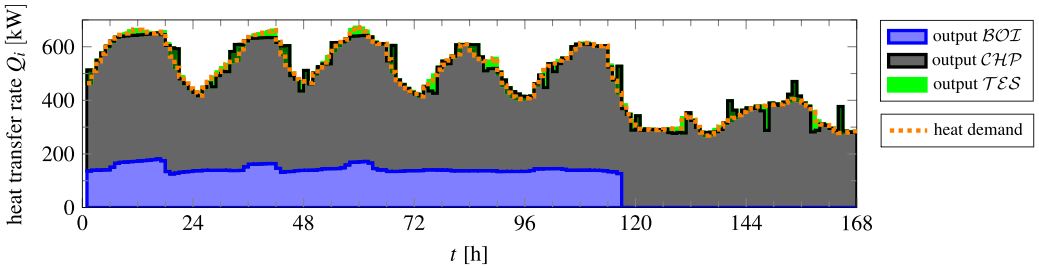

(a) Satisfaction of heating demand by CHP, boiler, and TES

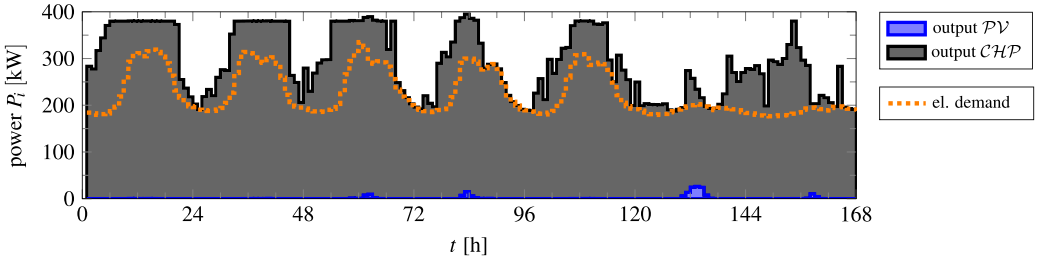

(b) Satisfaction of electricity demand by CHP and PV components

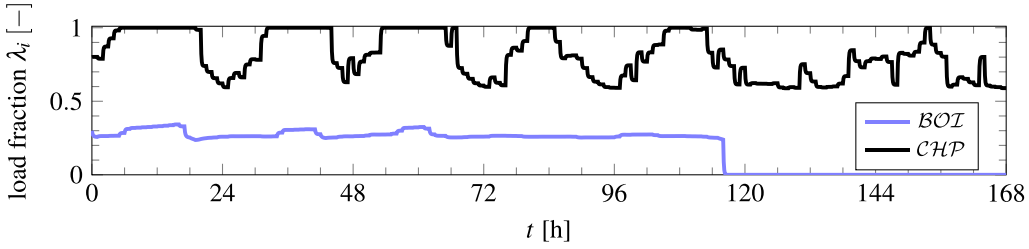

(c) Optimal part-load performance of boiler and CHP

Fig. 7. Optimal operation of an energy supply system for heating and electricity demands of 10 buildings. Note that the transfer rates in (a) and (b) are additive.

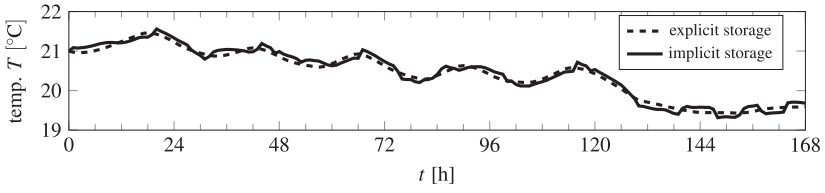

Fig. 8. Internal temperature of Building "OB1" based on simulated heat input and simulated heat input plus optimized heat transfer rate of TES

generation capabilities of the CHP are further exploited while the boiler drops instantaneously below its minimum load fraction and is therefore turned off.

Finally, we transfer the capability of the TES as explicit storage to Building "OB 1" as implicit storage. In particular, the optimized heat transfer rate interchanged with the TES Q_i, $i \in \mathcal{TES}$ is added to heating demand $Q^{\text{heat,dem}}$ given in B.2.2 which has been used for the dynamic optimization. The internal temperature within Building "OB 1" is simulated based on heat demand $Q^{\text{heat,dem}}$, i.e., for an energy system with an explicit storage only, and the combined demand $Q^{\text{heat,dem}} + Q_i$, $i \in \mathcal{TES}$, i.e., for an analogous energy system with an implicit storage only. Fig. 8 shows that the transfer of the heat transfer rate Q_i, $i \in \mathcal{TES}$ from the TES to Building "OB 1" leads to visible but for human hardly sensible oscillations in the range of up to 0.2K.

4. Conclusion

This article presents a model compendium for common components of energy supply systems present in industrial or research campus areas. Moreover, the included validated building models rely on real-world data from the Campus North of the Karlsruhe Institute of Technology and from the Forschungszentrum Jülich (HECI, 2019). We provide one model formulation on the scale of energy flow rates for each component considered. The model compendium is structured in terms of notation and modeling principles such that it can be extended by additional components, e.g., solar-thermal collectors and power-to-X technologies, or by including high-fidelity models, e.g., for gas grids and thermal grids.

The compendium addresses requirements of different fields of applications, namely the optimization of design, operation, and

control of energy supply systems. Hence, it includes both quasi-stationary and dynamic models as well as linearization schemes. The notation of all given models is unified for more transparency concerning synergies and structural differences of the different fields of applications. This way, we aim to support the transfer of models and methods between the different fields of applications. Moreover, the unified modeling framework allows investigating the influence of different formulations on computation times and on the accuracy of solutions. For instance, two corresponding optimization problems can be obtained for the same individual energy system by replacing the quasi-stationary model of one component by the respective dynamic model.

Additionally, we propose two optimization benchmarks exploiting the wide range of presented model formulations. In the first case study, a bi-criteria design optimization regarding total annual costs and global warming impact is performed for the generic energy system based on linearized quasi-stationary models. The results of the design optimization hint at the benefit of photovoltaic components, storage systems as well as the synergy of trigeneration for an ecological energy supply. In the second case study, the operational optimization of an energy supply system based on nonlinear dynamic models emphasizes the possibility to exploit varying electricity prices with the help of a combined heat and power engine and a thermal energy storage. For the sake of illustration, we also touch upon the role of thermal inertia of buildings via subsequent simulations. The case studies constitute substantial numerical challenges, e.g., for testing global solution methods for the operational optimization. Both can be easily adapted, e.g., to allow for different boundary conditions for the operation.

Notably, the benchmarks come with a complete set of ready-to-use input data and the respective model files, namely a GAMS (McCarl and Rosenthal, 2016) listing file for the design optimization and a Modelica (Mattsson and Elmqvist, 1997) file for the dynamic optimization of operation, available at https://git.es2050.org/heci/energy-benchmark. We also provide equivalent Pyomo files. The data sets may be extended by real-world measurements of demands and their corresponding price and weather data to account for model-plant-mismatch or real-world uncertainties.

The novelty of our approach is the definition of suitable benchmarks, writing consistent models for important unit operations allowing for various use cases, and combining these models with useful data. We utilize established solution methods and the models are not fundamentally different from existing state-of-the-art models. We envision the modular compendium, the nominal data set, and the benchmarks to enable transparent comparisons of optimization methods for sector-coupled energy systems.

Author Contribution

The author contribution possibility was offered after our submission.

Declaration of Competing Interest

We have no conflict of interest.

Acknowledgment

Dedication: This article is dedicated to Lotte who chose a dreamlike world.

Funding: This work was supported by the Helmholtz Association under the Joint Initiative “Energy System 2050 – A Contribution of the Research Field Energy”.

Susanne Sass is grateful for her association to the International Research Training Group (DFG) IRTG-2379 Modern Inverse Problems.

We are thankful to John Siirola for his helpful suggestions on Pyomo and to Bethany Nicholson for her help in converting Modelica to pyomo.dae.

Author Contributions: SS led and coordinated the writing to which all authors contributed. SS, TF, DEH, DS, and TS equally contributed to the model compendium. AB, LG, VH, DM, and AM guided the research of SS, DEH, DS, and TS. DS performed the parameter identification for the models of buildings and the corresponding simulation of demand data with input and guidance from LG. DEH performed case study “Design optimization” with input and guidance from AB. DYS prepared the publishable material. SS performed case study “Operational optimization” with input and guidance from AM. CK prepared the publishable material.

Appendix A. Notation

The variables, see Table A.1, are specified with the help of superscripts, see Table A.3, and assigned to certain sets via subscripts, see Table A.2. Apart from this, we omit explicit time-dependency in equations for the sake of simplicity unless it may create confusions. Thus, variables which depend explicitly on time are written in standard font, e.g., load fraction λ, while all other variables are represented by bold symbols, e.g., minimum load fraction $\boldsymbol{\lambda}^{\min}$ or efficiency $\boldsymbol{\eta}(\lambda)$. Whenever time-dependent variables occur in equations, these equations have to be satisfied at any considered time point $t \geq 0$.

Table A.1
List of variable and parameter symbols

Symbol	Unit	Description
$\boldsymbol{\beta}$	*context dependent*	slope of line segments used in linearization
γ	*context dependent*	miscellaneous parameters
$\boldsymbol{\epsilon}$	–	emissivity
$\boldsymbol{\eta}$	–	coefficient of performance or efficiency, resp.
$\boldsymbol{\vartheta}$	◦	inclination angle
θ	rad	phase angle of electrical voltage
$\lambda/\boldsymbol{\lambda}/l$	–	load fraction
$\boldsymbol{\rho}$	kgm^{-3}	density
$\boldsymbol{\sigma}$	$\mathrm{W\ m}^{-2}\ \mathrm{K}^{-4}$	Stefan Boltzmann constant
$\boldsymbol{\tau}$	s	time constant
$\boldsymbol{\phi}$	◦	azimuth orientation
$\boldsymbol{a}$	–	absorptivity
$\boldsymbol{A}$	m^2	area
b	–	indicator for active line segment
c	EUR/(kWh)	tariffs for purchasing/selling Energy
$\boldsymbol{C}$	JK^{-1}	heat capacity
d	W	auxiliary variable to linearize bilinear product
$E/\boldsymbol{E}$	kWh	(saved) energy
I	$\mathrm{W\ m}^{-2}$	solar irradiance
$m/\boldsymbol{m}$	kg	mass of working fluid
$\boldsymbol{M}$	$\mathrm{kg\ s}^{-1}$	mass flow rate
$P/\boldsymbol{P}$	W	electric power
$Q/\boldsymbol{Q}$	W	thermal energy flow rate
$T/\boldsymbol{T}$	K	temperature
$\boldsymbol{\Delta T}$	K	temperature difference
$\boldsymbol{V}$	m^3	volume
CAPEX	EUR	investment costs
gwi	$\mathrm{g}_{\mathrm{CO_2-eq.}}/\mathrm{kWh}$	global warming impact of energy source
GWI	$\mathrm{kg}_{\mathrm{CO_2-eq.}}/\mathrm{a}$	global warming impact of energy supply system
PVF	a^{-1}	present value factor
TAC	EUR/a	total annualized costs

Table A.2
List of sets and subscripts

Symbol	Description
$f \in \mathcal{F}$	set of mass flows
$j \in \mathcal{J}$	set of intervals for piece-wise linearization
$s \in \mathcal{S}$	set of building surfaces
$t \in \mathcal{T}$	set of time points
$z \in \mathcal{Z}$	set of thermal zones
$i \in \mathcal{C}$	set of conversion units, i.e., $\mathcal{C} = \mathcal{AC} \cup \mathcal{BOI} \cup \mathcal{CHP} \cup \mathcal{CC}$
$i \in \mathcal{G}$	set of generators in the electrical grid $\mathcal{G} \subseteq \mathcal{N}$
$i \in \mathcal{N}$	node set of the electrical grid
$i \in \mathcal{U}$	superset of all units of any component:
$i \in \mathcal{AC}$	set of absorption chiller units
$i \in \mathcal{BAT}$	set of battery units
$i \in \mathcal{BOI}$	set of boiler units
$i \in \mathcal{CC}$	set of turbo-driven compression chiller units
$i \in \mathcal{CHP}$	set of combined heat and power engine (CHP) units
$i \in \mathcal{HP}$	set of heat pump units
$i \in \mathcal{PV}$	set of photovoltaic (PV) units
$i \in \mathcal{TES}$	set of thermal energy storage units
$i \in \mathcal{WT}$	set of wind turbine units

Table A.3
List of superscripts

Symbol	Description
air	air
amb	ambient
cool	belonging to cooling grid / period
dem	demand
el	belonging to electric grid
gen	generation
heat	belonging to heating grid / period
in	input or inlet
irr	irradiance
k	concerning air exchange rate
lb	lower bound
loss	losses
max	maximum
min	minimum
nom	nominal
out	output or outlet
th	thermal (cooling or heating)
tot	total
U	concerning U value
ub	upper bound
0	reference value

Appendix B. Model compendium

In this section, economic and environmental evaluation criteria for design, operation, and control of a sector-coupled energy supply system as well as (non-)linear quasi-stationary and dynamic models are given for common components. This includes models for office buildings and experimental facilities; models for the conversion components boiler ($\mathcal{BOI}$), combined heat and power engine ($\mathcal{CHP}$), absorption chiller ($\mathcal{AC}$), turbo-driven compression chiller ($\mathcal{CC}$), and heat pump ($\mathcal{HP}$); models for photovoltaic units ($\mathcal{PV}$) and wind turbines ($\mathcal{WT}$) clustered as generation components; models for thermal energy storage ($\mathcal{TES}$) as well as batteries ($\mathcal{BAT}$); and, finally, models for the thermal and the electricity grid coupling these components.

The linearization scheme for the nonlinear efficiency curves and investment costs is given in Appendix C. Finally, an extension of the dynamic model of boiler and CHP for the inclusion of a minimum load fraction without the introduction of binaries or non-smoothness is given in Appendix D.

Table B.1
Parameter values of the conversion components taken from Baumgärtner et al. (2019)

Components	$\mathbf{CAPEX}_i^0/e$	$\gamma_{6,i}$
$\mathcal{BOI}$	2701.6	0.4502
$\mathcal{CHP}_1$	9332.6	0.539
$\mathcal{CHP}_2$	9332.6	0.539
$\mathcal{CHP}_3$	9332.6	0.539
$\mathcal{AC}$	8847.5	0.4345
$\mathcal{CC}$	444.3	0.8732
$\mathcal{PV}$	4264.3	0.9502
$\mathcal{HP}$	1654.7	0.6611
$\mathcal{TES}^{\text{cool}}$	57.5	0.9037
$\mathcal{TES}^{\text{heat}}$	83.8	0.8663
$\mathcal{BAT}$	2116.1	0.8382

B1. Evaluation criteria

In the following Sections B.1.1 and B.1.2 we introduce the total annualized costs **TAC** and the global warming impact **GWI** as evaluation criteria.

B1.1. Total annualized costs

Total annualized costs (TAC) are an economic criterion for the evaluation of an energy supply system with respect to operational, investment, and maintenance costs. The TAC can be calculated by

$$\mathbf{TAC} = \sum_{t\in\mathcal{T}} \Big[8760\,\text{h} \cdot \tau^{\text{dur}}(t) \cdot \Big(c^{\text{fuel}}(t) \cdot Q^{\text{fuel,in}}(t) + c^{\text{el,buy}}(t) \cdot P^{\text{buy}}(t) - c^{\text{el,sell}}(t) \cdot P^{\text{sell}}(t) \Big) \Big] + \sum_{i\in\mathcal{U}} \left(\frac{1}{\mathbf{PVF}} + \gamma_{4,i} \right) \cdot \mathbf{CAPEX}_i$$

with duration of time step $8760\,\text{h} \cdot \tau^{\text{dur}}$ per year τ^{dur}, prices $c^{\text{fuel}}, c^{\text{el,buy}}, c^{\text{el,sell}}$, purchased energy rate with respect to natural gas $Q^{\text{fuel,in}}$, purchased and sold electricity P^{buy} and P^{sell}, respectively, present value factor **PVF**, factor for maintenance costs per year $\gamma_{4,i}$, and capital expenditure $\mathbf{CAPEX}_i$.

The present value factor can be calculated by (Broverman, 2010)

$$\mathbf{PVF} = \frac{(\gamma_5 + 1)^{\tau^{\text{h}}} - 1}{(\gamma_5 + 1)^{\tau^{\text{h}}} \cdot \gamma_5}$$

with interest rate γ_5, e. g., $\gamma_5 = 8\,\%$, and time horizon τ^{h}, e. g., $\tau^{\text{h}} = 4\,\text{a}$. In this study, we obtain the CAPEX by the power law of capacity Smith (2005)

$$\mathbf{CAPEX}_i = \mathbf{CAPEX}_i^0 \cdot \left(\frac{\boldsymbol{Q}_i^{\text{nom}}}{Q_i^0} \right)^{\gamma_{6,i}}, \tag{B.1}$$

with reference capital expenditure $\mathbf{CAPEX}_i^0$ corresponding to the reference capacity Q_i^0 of 1kW, installed nominal capacity Q_i^{nom}, and the component dependent constant $\gamma_{6,i}$, see for example Table B.1. The linearization of the nonlinear power law (B.1) is explained in C.2.

Instead of the total annualized costs **TAC**, any other economic objective function could be chosen. However, when regarding economic and ecologic criteria, the total annualized costs **TAC** lead to Pareto fronts with low environmental impacts compared to other economic objective functions (Pintarič and Kravanja, 2015).

B1.2. Global warming impact

An environmental evaluation criterion of energy supply systems is given by its global warming impact

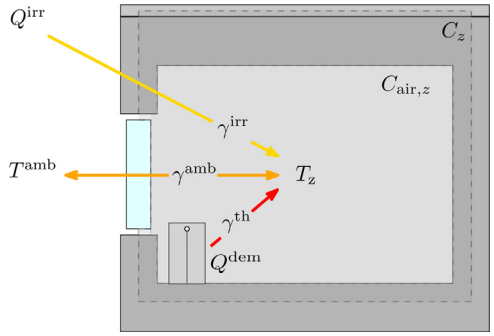

Fig. B.1. Heat flow scheme for building with relevant contributions

$$\mathbf{GWI} = \sum_{t\in\mathcal{T}} 8760\,\mathrm{h}\ \cdot\ \tau^{\mathrm{dur}}(t)\cdot \left[\mathbf{gwi}^{\mathrm{fuel}}\cdot Q^{\mathrm{fuel,in}}(t) + gwi^{\mathrm{el}}(t)\cdot\left(P^{\mathrm{in}}(t)-P^{\mathrm{out}}(t)\right)\right],$$

where $\mathbf{gwi}^{\mathrm{fuel}}$ and gwi^{el} are the specific global warming impacts of the energy sources, for example values see Section 3.1 or Federal Environment Office (2018). Note that the specific global warming impact of purchased electricity is varying remarkably over time. We follow the idea of the avoided burden (Baumann and Tillman, 2014) and assume a credit for the global warming impact **GWI** when electricity is fed into the grid. As the operation usually affects the global warming impact significantly higher than the manufacturing of the components (Guillén-Gosálbez, 2011), we only consider the contribution of the operation.

B2. Buildings

The models of buildings origin from the energy balance equation

$$\boldsymbol{C}_z\frac{\mathrm{dT_z}}{\mathrm{dt}} = Q_z^{\mathrm{in,tot}} - Q_z^{\mathrm{out,tot}} \tag{B.2}$$

based on the following assumptions:

(A1) Only internal energy is considered. In particular, the kinetic energy of the system is neglected and potential energy cancels out.
(A2) The change of internal energy equals the heat flow, i.e., no additional work is applied to the system.
(A3) The mass balance is fulfilled.

As sketched in Fig. B.1, the physical effects which most strongly influence the temperature within the buildings are identified as

(P1) Heat transport mechanisms with external air of temperature T^{amb} via air exchange based on air change rate $\boldsymbol{\gamma}_7^{\mathrm{amb,k}}$ and heat capacity $\boldsymbol{C}_{\mathrm{air},z}$ as well as heat transfer through walls, windows, roof, and floor based on heat transfer coefficient $\boldsymbol{\gamma}_7^{\mathrm{amb,U}}$,
(P2) Heat input by solar irradiance $Q_{s,z}^{\mathrm{irr}}$ on the building surface s with the solar energy absorption coefficient $\boldsymbol{\gamma}_8^{\mathrm{irr}}$ according to Harb et al. (2016), and
(P3) Installed heating/cooling system with heating/cooling input Q_z^{dem} with heating factor $\boldsymbol{\gamma}_9^{\mathrm{th}}$.
(P4) Heat capacity $\boldsymbol{C}_z$ takes into account internal walls, air, external walls, roof, and basement floor. However, it is only a fraction of the sum of all heat capacities $\boldsymbol{C}^{\mathrm{tot}}$ of the components of the building. This is presumably the case, since the outer shell is stronger coupled to the ambient temperature than to the inside and therefore does not significantly contribute to the indoor climate. Due to missing data, the verification of this hypothesis is subject to future work. The fraction $\frac{\boldsymbol{C}_z}{\boldsymbol{C}^{\mathrm{tot}}}$ is determined by the parameter identification in B.2.1 with $\boldsymbol{\gamma}_9^{\mathrm{th}}$ kept ≤ 1. When transferring the model to other buildings, a first approximation for $\boldsymbol{C}_z$ would be to calculate $\boldsymbol{C}^{\mathrm{tot}}$ of the new building multiplied by a ratio $\frac{\boldsymbol{C}_z}{\boldsymbol{C}^{\mathrm{tot}}}$ from Table B.3.

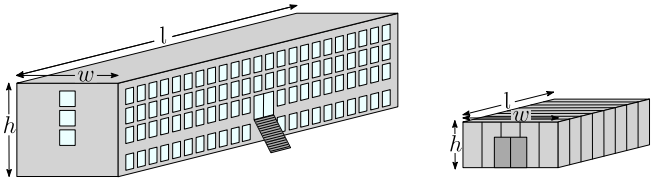

(a) Office building (b) Experimental facility

Fig. B.2. Dimensions of modeled buildings

Incorporating physical effects (P1) to (P4) into Eq. (B.2) yields a gray-box model equation for each thermal zone $z = 1, \ldots, n_z$, $n_z = \mathrm{card}(\mathcal{Z})$

$$\boldsymbol{C}_z\frac{\mathrm{dT_z}}{\mathrm{dt}} = (\boldsymbol{\gamma}_7^{\mathrm{amb}})_z\cdot\left(T^{\mathrm{amb}}-T_z\right) + \boldsymbol{\gamma}_8^{\mathrm{irr}}\sum_s\left(Q_{s,z}^{\mathrm{irr}}(\boldsymbol{A}_{s,z},\boldsymbol{\phi}_s)\right) + \boldsymbol{\gamma}_9^{\mathrm{th}}Q_z^{\mathrm{dem}} \tag{B.3}$$

with $(\boldsymbol{\gamma}_7^{\mathrm{amb}})_z = \boldsymbol{\gamma}_7^{\mathrm{amb,U}}\cdot\sum_{s\in\mathcal{S}_z}\boldsymbol{A}_s + \boldsymbol{\gamma}_7^{\mathrm{amb,k}}\cdot\frac{\boldsymbol{C}_{\mathrm{air,z}}}{3600\mathrm{s}}$
and $\mathcal{S}_z = \{\mathrm{east},\ \mathrm{south},\ \mathrm{west},\ \mathrm{north}\}\cup\{\mathrm{roof\ if\ contained\ by\ Zone\ z}\}\cup\{\mathrm{floor\ if\ contained\ by\ Zone\ z}\}$.

Eq. (B.3) provides a dynamic equation for differential state T_z in dependence of control input Q_z^{dem} as well as time-varying parameters T^{amb} and $Q_{s,z}^{\mathrm{irr}}$, $s\in\mathcal{S}$ for any thermal zone $z\in\mathcal{Z}$. Example values are given in Section B.2.1.

The model is based on Park et al. (2011). It is chosen to be as simple as reasonable for easy integration in different use cases and has been extended by considering solar irradiance. The parameter values given serve as first orientation for researchers without access to building models. It is generally advisable to estimate the parameters on data as the parameters vary depending on the characteristics of the buildings. The model can be adopted to different building sizes or orientations by changing the surface areas and the dependent solar irradiance. Moreover, in the case studies, we consider simple cuboid shape. If the shape of the building is different, it would be sensible to estimate the parameters to temperature measurements and/or explicitly take self-shading effects into consideration.

Note that parameter identification via linear regression of averaged measurement data of the indoor temperature shows that the consideration of additional factors like human body heat, electrical devices, wind velocity, coupling between different zones, and wall temperatures leads to worse identification results due to linear dependencies displayed by high condition numbers.

B2.1. Parameter identification

The parameters $(\boldsymbol{\gamma}_7^{\mathrm{amb}})_z$, $\boldsymbol{\gamma}_8^{\mathrm{irr}}$, and $\boldsymbol{C}_z$ of the gray-box model are fitted to measured temperature data T_z with $\boldsymbol{\gamma}_9^{\mathrm{th}}\leq 1$ and the input time series T^{amb}, Q_z^{dem}, and $Q_{s,z}^{\mathrm{irr}}$. In fact, dimensions and common information of the two original buildings, the office building "OB 1" and the experimental facility "EF 1", are retrieved from internal reports as shown in Fig. B.2 and Table B.2.

Moreover, ambient temperature T^{amb} is given by weather data of year 2018 from Deutscher Wetterdienst for Stuttgart (DWD Climate Data Center (CDC), 2018). Solar irradiance I_s is calculated using the horizontal global irradiance and the horizontal diffuse irradiance of the weather data as well as considering the orientation

Table B.2
Common information of modeled buildings and virtual PV, cf. B.4.1

Attribute	Off. bldg. (OB)	Off. bldg. mod. (OBM)	Exp. fac. (EF)
Construction year	1973	1973	2011
Orientation $\boldsymbol{\phi}_{\text{north}}$	13°	13°	13°
Position	N49°5′43.9872", E8°26′1.2451"		
Stories	4	3	1
Width w [m]	12.6	12.6	12.2
Height h [m]	13.3	10.1	5.9
Length l [m]	61.4	61.4	20.0
Heat capacity air $\boldsymbol{C}^{\text{air}}$ $[MWsK^{-1}]$	11.4	8.7	1.8
$T_z^{\max}$ Winter [°C]	24	24	24
$T_z^{\min}$ Winter [°C]	18	18	16
$T_z^{\max}$ Summer [°C]	26	26	26
$T_z^{\min}$ Summer [°C]	20	20	18
Orientation $\boldsymbol{\phi}^{\text{PV}}$	half of the units 103°, other half 283°		193°
Inclination $\boldsymbol{\vartheta}^{\text{PV}}$		10°	30°

Table B.3
Parameters of buildings

Building	$\boldsymbol{C}_z$ [MW s/K]	$\frac{\boldsymbol{C}_z}{\boldsymbol{C}^{\text{tot}}}$ [–]	$\boldsymbol{\gamma}_7^{\text{amb}}$ [W/K]	$\boldsymbol{\gamma}_7^{\text{amb,U}}$ [W/(m^2 K)]	$\boldsymbol{\gamma}_7^{\text{amb,k}}$ [–]	$\boldsymbol{\gamma}_8^{\text{irr}}$ [–]	$\boldsymbol{\gamma}_9^{\text{th}}$ [–]	$\boldsymbol{Q}_z^{\text{dem,max}}$ [kW]
OB 1	1530.4	0,529	3651	0,545	0,545	0.037	1	100
OB 2	1607,3	0,556	4789	0,611	0,833	0.033	1	100
OB 3	1446.5	0.500	5015	0,750	0,750	0.045	1	100
OB 4	1522.7	0.526	3480	0,658	0,368	0.037	1	100
OB 5	1701.8	0.588	4326	0,647	0,647	0.047	1	100
OB 6	1522.7	0.526	2833	0,474	0,368	0.037	1	100
OBM 1	1201.1	0.526	3450	0,632	0,632	0.037	1	80
OBM 2	1267.9	0.556	3872	0,611	0,833	0.033	1	80
EF 1	98.5	0,443	713	0,518	0,518	0.053	1	18
EF 2	98.5	0,443	671	0,487	0,487	0.049	1	18

of each surface $s \in \mathcal{S}$ by angle $\boldsymbol{\phi}_s$ according to Kreider et al. (2010). The two original buildings have no solar panels installed, therefore possible shading effects are neglected. Finally, solar heat input $Q_{s,z}^{\text{irr}}$ is the product of solar irradiance I_s and the respective area $\boldsymbol{A}_{s,z}$ for any surface $s \in \mathcal{S}$ and thermal zone $z \in \mathcal{Z}$.

The values resulting from the parameter identification process with one thermal zone are given in Table B.3. Note that the parameters for buildings "OB 1" and "EF 1" are identified based on real measurement data. For the parameters of "OB 2" to "OB 6" as well as "OBM 1" and "OBM 2", intervals are predefined according to empirical considerations. Their parameters approximately follow a uniform distribution within those intervals. The parameters of "EF 2" are slight variations of those of "EF 1". The following Section B.2.2 depicts the simulation of the heating/cooling demand.

Table B.4
Control parameters of buildings

Building	$\boldsymbol{T}^{0,\text{cool}}$ [°C]	$\boldsymbol{T}^{0,\text{heat}}$ [°C]	NS [–]	WES [–]	$\boldsymbol{\gamma}_{10}$ [kW/K]	$\boldsymbol{\gamma}_{11}$ [W/(K s)]
OB 1	23	21	true	true	100	0
OB 2	23	22	true	true	100	0.1
OB 3	24	20	false	true	100	0
OB 4	23	21	true	false	100	0
OB 5	23	22	true	true	100	0
OB 6	23	23	false	false	100	0
OBM 1	23	21	true	true	100	0
OBM 2	23	22	true	true	100	0.1
EF 1	23	18	true	false	10	0,2
EF 2	21	19	false	false	10	0,2

B2.2. Simulation of building demands

For simulating realistic building demands[3], the common approach of a standard PI controller representing a thermostat is used for the control of the buildings (Peeters et al., 2008). The deviation from desired temperature $\boldsymbol{T}^0$ is the input. The feedback loop for any thermal zone $z \in \mathcal{Z}$ is defined by

$$Q_z^{\text{dem}} = \text{sat}_{\boldsymbol{Q}_z^{\text{lb}}}^{\boldsymbol{Q}_z^{\text{ub}}}\left(\boldsymbol{\gamma}_{10,z}\left(T_z - \boldsymbol{T}_z^0\right) + \boldsymbol{\gamma}_{11,z}\int_0^t \left(T_z(\tau) - \boldsymbol{T}_z^0\right)\mathrm{d}\tau\right)$$

with saturation

$$\text{sat}_{\boldsymbol{Q}^{\text{lb}}}^{\boldsymbol{Q}^{\text{ub}}}(u) = \begin{cases} \boldsymbol{Q}_z^{\text{ub}}, & \text{if} \quad u > \boldsymbol{Q}_z^{\text{ub}} \\ u, & \text{if} \quad \boldsymbol{Q}_z^{\text{lb}} \le u \le \boldsymbol{Q}_z^{\text{ub}} \\ \boldsymbol{Q}_z^{\text{lb}}, & \text{if} \quad u < \boldsymbol{Q}_z^{\text{lb}} \end{cases}.$$

[3] These demands are often referred to as building loads in the community for modeling, simulation, and optimization of buildings.

For control and optimization, the internal temperatures have to stay within comfort zones $T_z^{\min} \le T_z \le T_z^{\max}$ and the heating/cooling input within its technical limitations $0 \le |Q_z^{\text{dem}}| \le Q_z^{\text{dem,max}}$. Table B.4 provides the controller gains $\boldsymbol{\gamma}_{10,z}$ for the proportional term and $\boldsymbol{\gamma}_{11,z}$ for the integral term as well as the used reference temperatures $\boldsymbol{T}_z^0$. If the parameter night shift (NS) is true, the temperature set point is changed by +1K during the night in cooling periods and −1K during the night in heating periods. Similarly, if the parameter weekend shift (WES) is true, the temperature set point is changed ± 1K on weekends and holidays. The saturation bounds are given by $\boldsymbol{Q}_z^{\text{ub}^{\text{winter}}} = \boldsymbol{Q}_z^{\text{dem,max}}$, $\boldsymbol{Q}_z^{\text{lb}^{\text{winter}}} = \boldsymbol{Q}_z^{\text{ub}^{\text{summer}}} = 0$, and $\boldsymbol{Q}_z^{\text{lb}^{\text{summer}}} = -\boldsymbol{Q}_z^{\text{ub}^{\text{winter}}}$.

Both electrical and thermal demand of a campus consisting of 6 office buildings of type "OB", 2 smaller office buildings of type "OBM" (office building modified), and 2 experimental facilities "EF" are simulated based on Eq. (B.3) and the model parameters discussed in B.2.1, see Fig. B.3. Note that the heating demand is given

Table B.5
Example values for efficiency and COP curves of the considered conversion components

Formula and values	Reference
Boiler $i \in \mathcal{BOI}$	
$\eta_i^{\text{heat}}(\lambda_i) = \frac{21.75378 \cdot \lambda_i^3 - 7.00130 \cdot \lambda_i^2 + 1.39731 \cdot \lambda_i - 0.07557}{20.66646 \cdot \lambda_i^3 - 5.34196 \cdot \lambda_i^2 + 0.67774 \cdot \lambda_i + 0.03487} \cdot \eta_i^{\text{nom,heat}}$	Voll (2013) based on Fabrizio (2008)
$\eta_i^{\text{nom,heat}} = 0.8$	Voll (2013)
Combined heat and power engine $i \in \mathcal{CHP}$	
$\eta_i^{\text{heat}}(\lambda_i) = \left(-0.0768 \cdot \lambda_i^2 - 0.0199 \cdot \lambda_i + 1.0960\right) \cdot \eta_i^{\text{nom,heat}}(\boldsymbol{Q}_i^{\text{nom}})$	Approx. to producer information
$\eta_i^{\text{el}}(\lambda_i) = \left(-0.2611 \cdot \lambda_i^2 + 0.6743 \cdot \lambda_i + 0.5868\right) \cdot \eta_i^{\text{nom,el}}(\boldsymbol{Q}_i^{\text{nom}})$	Approx. to producer information
$\eta_i^{\text{nom,heat}}(\boldsymbol{Q}_i^{\text{nom}}) = -3.55 \cdot 10^{-5} \cdot \frac{\boldsymbol{Q}_i^{\text{nom}}}{1\text{kW}} + 0.498$	Voll (2013)
$\eta_i^{\text{nom,el}}(\boldsymbol{Q}_i^{\text{nom}}) = 3.55 \cdot 10^{-5} \cdot \frac{\boldsymbol{Q}_i^{\text{nom}}}{1\text{kW}} + 0.372$	Voll (2013)
$\eta^{\text{nom,tot}} = 0.87$	Voll (2013)
Heat pump $i \in \mathcal{HP}$	
$\eta_i^{\text{heat}}(\lambda_i) = 0.36/\eta^{\text{carnot}}$	Approx. to data sheet Dimplex (2019)
$\eta^{\text{carnot}} = 1 - \frac{T}{\boldsymbol{T}_{\mathcal{HP}}}$; $\boldsymbol{T}_{\mathcal{HP}} = 273.15 + 60\text{K}$	
Absorption chiller $i \in \mathcal{AC}$	
$\eta_i^{\text{cool}}(\lambda_i) = \frac{\lambda_i}{0.83330 \cdot \lambda_i^2 - 0.08330 \cdot \lambda_i + 0.24999} \cdot \eta_i^{\text{nom,cool}}$	Voll (2013) based on Fabrizio (2008)
$\eta_i^{\text{nom,cool}} = 0.67$	Voll (2013)
Turbo-driven compression chiller chiller $i \in \mathcal{CC}$	
$\eta_i^{\text{cool}}(\lambda_i) = \left(0.8615 \cdot \lambda_i^3 - 3.5494 \cdot \lambda_i^2 + 3.6790 \cdot \lambda_i + 0.0126\right) \cdot \eta_i^{\text{nom,cool}}$	Voll (2013)
$\eta_i^{\text{nom,cool}} = 5.54$	Voll (2013)

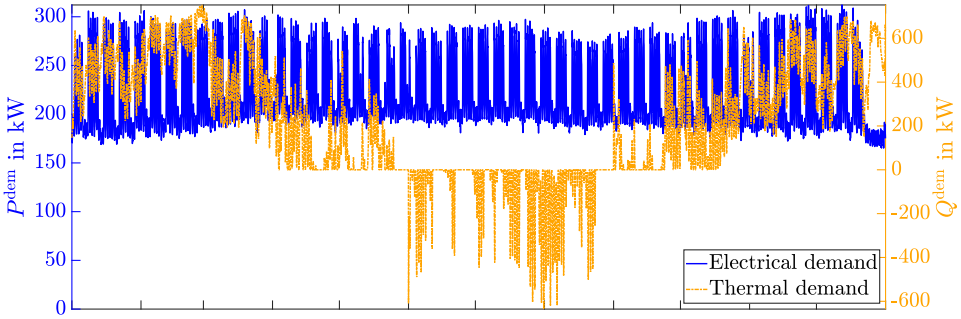

(a) Aggregated demand data of OB 1 to 6 and OBM 1 and 2

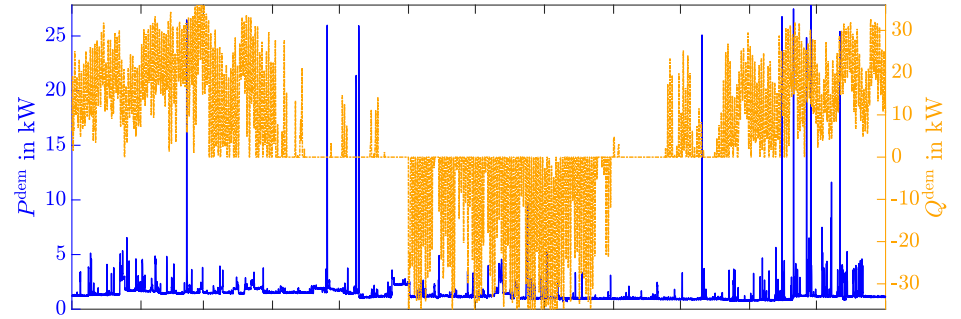

(b) Aggregated demand data of EF 1 and 2

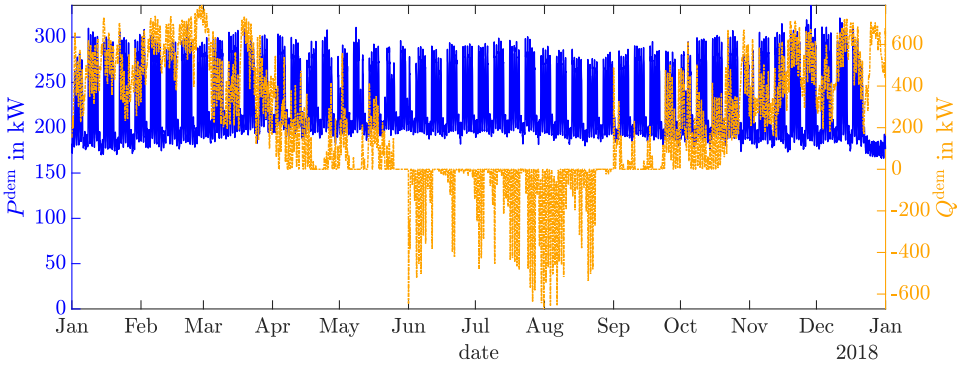

(c) Sum of data in Figures 11(a) and 11(b)

Fig. B.3. Aggregated demand data for the different types of buildings and a complete campus

by positive thermal demand values and the cooling demand by the absolute of the negative thermal demand values.

The aggregated electrical demand profile for the ten buildings is the sum of 1) three generated demand profiles following the G0 demand profile of BDEW (2019) with Saturdays treated like Sundays as well as different offsets and gains for each demand profile for three OB/OBM buildings; 2) measured data of "OB 1" for the years 2014 to 2018 which are shifted to start at the same day of week in order to retrieve five more OB/OBM demand profiles; and 3) measured data of "EF 1" for the years 2017 and 2018 to get two demand profiles for the EF buildings.

Weather and demand data ("WeatherAndDemandTimeSeries.csv") as well as the data shown in Figs. 2 and 3 ("ComparisonMeasSimTimeSeries.csv") are available at https://git.es2050.org/heci/energy-benchmark in directory "App_Weather_And_Demand".

B3. Conversion components

The quasi-stationary model for general conversion components $\mathcal{C} = \mathcal{BOI} \cup \mathcal{CHP} \cup \mathcal{HP} \cup \mathcal{AC} \cup \mathcal{CC}$ is given as in Voll et al. (2013) by

$$Q_i^{\text{out}} = \boldsymbol{\eta}_i^{\text{heat/cool}}(\lambda_i) \cdot Q_i^{\text{in}} \quad \forall\, i \in \mathcal{C} \setminus \mathcal{HP}\,, \tag{B.4a}$$

$$Q_i^{\text{out}} = \boldsymbol{\eta}_i^{\text{heat}}(\lambda_i) \cdot P_i^{\text{in}} \quad \forall\, i \in \mathcal{HP}\,, \tag{B.4b}$$

$$P_i^{\text{out}} = \boldsymbol{\eta}_i^{\text{el}}(\lambda_i) \cdot Q_i^{\text{in}} \quad \forall\, i \in \mathcal{CHP}\,, \tag{B.4c}$$

$$Q_i^{\text{out}} = \lambda_i \cdot \boldsymbol{Q}_i^{\text{nom}} \quad \forall\, i \in \mathcal{C}\,, \tag{B.4d}$$

$$\boldsymbol{\lambda}_i^{\min} \le \lambda_i \le 1 \quad \forall\, i \in \mathcal{C}\,, \tag{B.4e}$$

$$\boldsymbol{Q}_i^{\min} \le \boldsymbol{Q}_i^{\text{nom}} \le \boldsymbol{Q}_i^{\max} \quad \forall\, i \in \mathcal{C}\,, \tag{B.4f}$$

with energy balances based on respective efficiencies (B.4a) to (B.4c), Eq. (B.4d) determining load fraction λ, bounds (B.4e) and (B.4f). Note that $\boldsymbol{\eta}$ is the efficiency for boilers and CHPs, while it is the coefficient of performance (COP) for chillers and heat pumps.

For obtaining a dynamic model, Eq. (B.4a) can be replaced by

$$\frac{\mathrm{d}\lambda_i}{\mathrm{dt}} = \frac{1}{\boldsymbol{\tau}_i} \cdot \left(\boldsymbol{\eta}_i^{\text{heat/cool}}(\lambda_i) \cdot \frac{Q_i^{\text{in}}}{\boldsymbol{Q}_i^{\text{nom}}} - \lambda_i \right) \qquad \forall\, i \in \mathcal{C}\,, \tag{B.5}$$

see Sass and Mitsos (2019) for more details. Note that this dynamic model is based on a simplified energy balance that considers heat transfer rates rather than temperatures. Furthermore, all heat losses are assumed to be proportional to the input heat transfer rate.

The efficiency or COP curves $\boldsymbol{\eta}$ of the respective components are given in Table B.5. Note that the given curves are used for both the quasi-stationary and the dynamic models. Apart from this, all efficiency and COP curves are assumed to be temperature independent, which is reasonable for boilers and CHPs but not necessarily for chillers and heat pumps (Augenstein et al., 2005).

B4. Generation components

In the context of this article, the output of generation components is limited by their capacity and the availability of renewable energy resources, namely solar irradiation and wind. However, the maximum available power may not be exploited, e.g., if this would impair grid stability or exceed storage capabilities.

B4.1. Photovoltaic units

The electrical power P_i provided by a photovoltaic (PV) unit $i \in \mathcal{PV}$ is limited by the solar irradiance I, the total area $\boldsymbol{A}_i$ of the unit and its efficiency $\boldsymbol{\eta}_i$ via

$$P_i \le \boldsymbol{A}_i \cdot \boldsymbol{\eta}_i \cdot I, \quad i \in \mathcal{PV}\,.$$

Thereby, I accounts for direct, diffuse, and reflected solar irradiance onto the tilted PV unit's area.

Furthermore, the PV unit cannot exceed its nominal capacity

$$P_i \le \boldsymbol{A}_i \cdot P_i^{\text{nom}}, \quad i \in \mathcal{PV}\,,$$

where the nominal capacity depends on the area of the unit as well (Ren et al., 2009).

The average and maximum efficiency of current German PV technologies are 17% and larger than 20%, respectively, while the average performance ratio ranges from 80 to 90% (Wirth and Schneider, 2019). Thus, we choose efficiency $\boldsymbol{\eta}_i = 0.19$ and nominal capacity $P_i^{\text{nom}} = 0.171\text{kWm}^{-2} \cdot \boldsymbol{A}_i$ as an example.

For the case studies, the PV components are virtually installed on the roofs of the buildings described in B.2 with the parameters given in Table B.2. To avoid self-shading effects of the panels, it is assumed that the rows have a minimum distance of three times the (projected) height of the units. Thus, for an inclination of 30° the maximum available PV surface area is 42% of the total roof area, provided that the complete width of the roof can be used to install the panels. Applying that rule to the two experimental facility buildings, we have $\boldsymbol{A}_{\text{EF}}^{\max} \approx 205\text{m}^2$. The PV area for the office buildings is up to 85% of the total roof surface, i.e. $\boldsymbol{A}_{\text{OB}\cup\text{OBM}}^{\max} \approx 5261\text{m}^2$, since the inclination is only 10°. The irradiance I is calculated as described in Section B.2.1. The data is included in WeatherAndDemandTimeSeries.csv available at https://git.es2050.org/heci/energy-benchmark in directory "App_Weather_And_Demand".

B4.2. Wind turbine

The maximum power output of a wind turbine is determined by the wind velocity, which corresponds to the part-load behavior of the wind turbine, and its nominal capacity. We introduce efficiency $\boldsymbol{\eta}_{\mathcal{WT}}^{\text{el}}(\lambda_i)$ for the mapping of wind velocity to the power output for each wind turbine $i \in \mathcal{WT}$ and, thus, obtain

$$P_i^{\text{out}} \le \boldsymbol{\eta}_i^{\text{el}}(\lambda_i) \cdot P_i^{\text{nom}} \qquad \forall\, i \in \mathcal{WT}\,.$$

As an example, the efficiency

$$\boldsymbol{\eta}_i^{\text{el}}(\lambda_i) = \begin{cases} 0 & \forall\, \lambda_i \le 0.33 \\ 1.5393 \cdot \lambda_i - 0.5091 & \forall\, 0.33 \le \lambda_i \le 1.00 \\ 1 & \forall\, \lambda_i \ge 1.00 \end{cases} \tag{B.6}$$

given by ENERCON (2015) may be used. Thereby, load fraction λ_i is the wind velocity at each time step, normalized by the rated wind velocity, e.g. 15 m/s.

B5. Storage components

B5.1. TES

In this article, we only take into account a lumped model of a hot/cold water storage tank for the thermal energy storage (TES). More sophisticated multi-layer tank models are discussed in, e.g., Steen et al. (2015); Schütz et al. (2015).

The energy balance based on heat transfer rates of such a simple TES model yields

$$\begin{aligned} \frac{\mathrm{dE_i}}{\mathrm{dt}} &= \boldsymbol{\eta}_i^{\text{in}}\, Q_i^{\text{in}} - \frac{1}{\boldsymbol{\eta}_i^{\text{out}}}\, Q_i^{\text{out}} - \frac{1}{\boldsymbol{\tau}_i^{\text{loss}}}\, E_i \qquad && \forall i \in \mathcal{TES} \\ E_i(0) &= E_{i,0} && \forall i \in \mathcal{TES}\,. \end{aligned} \tag{B.7}$$

with added and withdrawn heat transfer rates Q_i^{in} and Q_i^{out}, respectively, efficiencies η_i^{in} and η_i^{out} as well as self-discharge in dependence of the currently stored energy E_i with time constant τ_i^{loss}. As an example, constant values $\tau_i^{\text{loss}} = 200\,\text{h}$ for the time constant of the heat loss and $\eta_i^{\text{in}} = \frac{1}{\eta_i^{\text{out}}} = 0.95$ for the efficiencies may be chosen. If input and output efficiencies coincide

$$\eta_i := \eta_i^{\text{in}} = \frac{1}{\eta_i^{\text{out}}}\,,$$

as in our example, input and output heat transfer rate can be aggregated, e.g., by $Q_i := Q_i^{\text{in}} - Q_i^{\text{out}}$. Thus, Eq. B.7 can be reformulated as

$$\frac{\text{dE}_\text{i}}{\text{dt}} = \eta_i\, Q_i - \frac{1}{\tau_i^{\text{loss}}}\, E_i \quad \forall i \in \mathcal{TES} \tag{B.8}$$

With reformulation Eq. (B.8) the number of degrees of freedom is reduced, since only the total heat transfer rate flowing through the thermal energy storage is considered. Note that the dynamics in Eq. (B.7) are commonly discretized using the implicit (Schütz et al., 2017) or explicit Euler scheme (Bahl et al., 2018b). However, in benchmark case study "Operational optimization" we stick to formulation Eq. (B.8), since a more sophisticated integration scheme is incorporated in the dynamic optimization framework used. Aside from that, binary variables can be introduced to prevent simultaneous charging and discharging, cf. battery model in Section B.5.2. The storage tank's capacity E_i^{nom} serves as an upper bound for the TES and presents a design variable determining its capacity

$$0 \le E_i \le E_i^{\text{nom}} \qquad \forall i \in \mathcal{TES}\,. \tag{B.9}$$

In the design optimization, capacity E_i^{nom} is limited by

$$E_i^{\text{min}} \le E_i^{\text{nom}} \le E_i^{\text{max}} \qquad \forall i \in \mathcal{TES}\,. \tag{B.10}$$

Moreover, the heat transfer rates for charging and discharging the TES are limited by

$$0 \le Q_i^{\text{in}} \le \frac{1}{\tau^{\text{in}}} E_i^{\text{nom}} \quad \forall i \in \mathcal{TES} \tag{B.11}$$

$$0 \le Q_i^{\text{out}} \le \frac{1}{\tau^{\text{out}}} E_i^{\text{nom}} \quad \forall i \in \mathcal{TES} \tag{B.12}$$

with rates $1/\tau^{\text{in}}$ and $1/\tau^{\text{out}}$ limiting the charging and discharging process, respectively. Appropriate values are given by $1/\tau^{\text{in}} = 1/\tau^{\text{out}} = 1\text{h}^{-1}$, cf. (Bahl et al., 2018b).

B5.2. Battery

A generic model of an electrical battery is given by replacing the heat transfer rates in Eq. (B.7) by the electrical power applied to the battery. However, self-discharge is often negligible for (Li-Ion) batteries (Zimmerman, 2004). This yields for any battery $i \in \mathcal{BAT}$

$$\begin{aligned} \frac{\text{dE}_\text{i}}{\text{dt}} &= \eta_i^{\text{in}} P_i^{\text{in}} + \frac{1}{\eta_i^{\text{out}}} P_i^{\text{out}} && \forall i \in \mathcal{BAT} \\ E_i(0) &= E_{i,0} && \forall i \in \mathcal{BAT}\,. \end{aligned} \tag{B.13}$$

As an example, we choose values $\eta_i^{\text{in}} = 0.920 \approx \eta_i^{\text{out}} = 0.926$ based on Baumgärtner et al. (2019) and the round-trip efficiency reported in Tesla (2019).

Constraints Eqs. (B.9) to (B.12) apply analogously to the battery model if heat transfer rate Q is swapped with power P where applicable. In contrast to a TES, the charging and discharging process of batteries is typically not limited by rate constraints. Baumgärtner et al. (2019) report time constants $\tau^{\text{in}} = \tau^{\text{out}} = 4.2 \cdot 10^{-5}$ h, which lead to large upper bounds in Eqs. (B.11) and (B.12). Note that the constraints implied by underlying power electronics are usually considerably tighter.

Similar to the case of TES models, cf. Section B.5.1, it is quite common to consider the discrete-time counter part of Eq. (B.13) in scheduling of power systems. To this end, the ODE can be discretized by the forward Euler method considering averaged values of $P^{\text{in}}(t)$ and $P^{\text{out}}(t)$ and a constant step width of e.g. 15min. We remark that the given model does not account for specifics of all existing battery technologies. For example, detailed models for RedOx-Flow (Blanc and Rufer, 2008) and other battery types are beyond the scope of this work.

In contrast to TES models, a battery cannot be charged and discharged at the same time. Put differently, the battery cannot actively *dissipate* energy. Hence, the constraint

$$P_i^{\text{in}} \cdot P_i^{\text{out}} = 0, \quad \forall i \in \mathcal{BAT}$$

is added. As this constraint leads to feasible sets with non-differentiable boundaries, it has been suggested to either neglect it (Braun et al., 2018), or to relax it as follows

$$P_i^{\text{in}} \cdot P_i^{\text{out}} = \varepsilon > 0, \quad \forall i \in \mathcal{BAT},$$

see e.g. Appino et al. (2018) for details.

Alternatively, one may model the asymmetric charging and discharging efficiencies by means of integer decision variables. Murray et al. (2018) proposed a mixed-integer formulation based on

$$1 - \eta_i^{\text{in}} = \frac{1}{\eta_i^{\text{out}}} - 1 = \eta_i \quad \forall i \in \mathcal{BAT}\,, \tag{B.14}$$

which is a common assumption for batteries in the literature in place of $\eta_i^{\text{in}} = \eta_i^{\text{out}}$. Substitution of (B.14) into (B.13) gives

$$\frac{\text{dE}_\text{i}}{\text{dt}} = (1 - \eta_i) P_i^{\text{in}} + (1 + \eta_i) P_i^{\text{out}} \quad \forall i \in \mathcal{BAT}\,.$$

The integer variable $z_i \in \{-1, 1\}$ allows to discriminate charging and discharging. Together with aggregating input and output, the following mixed-integer formulation

$$\frac{\text{dE}_\text{i}}{\text{dt}} = (1 + z_i \eta_i) P_i, \quad \forall z_i \in \{-1, 1\},\ i \in \mathcal{BAT}$$

is obtained.

B6. Grid models

We consider thermal, electricity, and gas grids as components and use simple models. In particular, gas is only a potential energy resource and the gas grid is approximated as a point source with a known gas price.

B6.1. Thermal grid

We do not consider an external thermal grid. Thus, cooling and heating supply have to match the aggregation of building demands and storage capacities.

According to Mehleri et al. (2012), an energy balance is formulated for each node j of the thermal grid, comprising generation, consumption, storage, and interaction with neighboring nodes l. For a given energy supply system, this results in

$$\begin{aligned} &\sum_{i \in \mathcal{BOI} \cup \mathcal{CH} \mathcal{P} \cup \mathcal{TES}^{\text{heat}}} Q_{i,j}^{\text{heat,out}} + \sum_l \left(\gamma_{l \to j}^{\text{heat}} \cdot Q_{l \to j}^{\text{heat}} - Q_{j \to l}^{\text{heat}} \right) \\ &= Q_j^{\text{heat,dem}} + \sum_{k \in \mathcal{AC} \cup \mathcal{TES}^{\text{heat}}} Q_{k,j}^{\text{heat,in}} \end{aligned}$$

for each node j of the heating grid and

$$\begin{aligned} &\sum_{i \in \mathcal{AC} \cup \mathcal{CC} \cup \mathcal{TES}^{\text{cool}}} Q_{i,j}^{\text{cool,out}} + \sum_l \left(\gamma_{l \to j}^{\text{cool}} \cdot Q_{l \to j}^{\text{cool}} - Q_{j \to l}^{\text{cool}} \right) \\ &= Q_j^{\text{cool,dem}} + \sum_{k \in \mathcal{TES}^{\text{cool}}} Q_{k,j}^{\text{cool,in}} \end{aligned}$$

for each node j of the cooling grid, where parameter $\boldsymbol{\gamma}$ is a loss factor. Mehleri et al. (2012) and Obara (2007) further approximate the loss factor $\boldsymbol{\gamma}$ proportional to the distance to the neighboring node l.

B6.2. Electricity grid

A simplified model of a balanced electrical AC (alternating current) grid can be given by a lumped-parameter system at steady-state, which can be described by the triple $(\mathcal{N}, \mathcal{G}, Y)$, where $\mathcal{N} = \{1, \ldots, N\}$ is the set of buses (nodes), $\mathcal{G} \subseteq \mathcal{N}$ is the non-empty set of generators, and $\boldsymbol{Y} = \boldsymbol{G} + \mathrm{j}\boldsymbol{B} \in \mathbb{C}^{N\times N}$ is the bus admittance matrix (Grainger and Stevenson, 1994). The off-diagonal entries of $\boldsymbol{Y}$ can be written as $\boldsymbol{y}_{li} = \boldsymbol{g}_{li} + \mathrm{j}\boldsymbol{b}_{li}$, whereby $\boldsymbol{g}_{li}$ is the conductance for the line li, respectively, $\boldsymbol{b}_{li}$ is the line susceptance. The diagonal entries of Y are $y_{ll} = y_l + \sum_{l\neq m} y_{li}$, where y_l accounts for linear load connected to bus l.

For the sake of simplicity, we assume that there is only one generator per bus (i.e. $\mathcal{G} \subseteq \mathcal{N}$). Thus, at each bus $i \in \mathcal{N}$ we have

$$P_i = P_i^{\mathrm{dem}} + P_i^{\mathrm{gen}} ,$$

where by convention $P_i^{\mathrm{gen}} = 0$ if $i \notin \mathcal{G}$. The parameter P_i^{dem} models the demand of electrical power at node i, it also captures uncontrollable renewable generation, e.g., the maximum power output of PV components. Batteries are considered to be generators.

To reduce nonconvexities, lossless lines, small phase differences, and constant voltage magnitudes are commonly assumed. With these assumptions, the overall active power balance for the grid reads

$$\sum_{i\in\mathcal{N}} P_i = 0. \tag{B.15}$$

Note that power balance Eq. (B.15) is used in the given benchmark case studies.

A simple expression for the phase angles θ_i at each bus is given by

$$P = -\sum_{i\in\mathcal{N}\setminus\{l\}} \boldsymbol{b}_{li}(\theta_l - \theta_i) \quad \Longleftrightarrow \quad P = -\boldsymbol{B}\theta \ , \tag{B.16}$$

where B is the imaginary part of the bus admittance matrix Y, P is the vector of electrical powers, and θ is the vector of phase angles. The above Eqs. (B.16) are the so-called DC (direct current) power flow equations (Grainger and Stevenson, 1994).

Appendix C. Linearization scheme

C1. Linearization of efficiency/COP curves

In this article, we assume that efficiency or COP $\boldsymbol{\eta}_i$ is a given, possibly nonlinear function in dependence of load fraction $\lambda_i := Q_i^{\mathrm{out}}/\boldsymbol{Q}_i^{\mathrm{nom}}$, see Table B.5. According to Voll et al. (2013), it is favorable to linearize the functional dependency of input heat transfer rate Q_i^{in} on output heat transfer rate Q_i^{out}

$$Q_i^{\mathrm{in}} = \frac{Q_i^{\mathrm{out}}}{\eta_i(\lambda_i)} = \frac{\lambda_i}{\eta_i(\lambda_i)} \cdot \boldsymbol{Q}_i^{\mathrm{nom}} \tag{C.1}$$

Table C.1
Supporting points of part-load behavior

Components	$\boldsymbol{\lambda}_{i,1}^{\mathrm{in}}$	$\boldsymbol{\lambda}_{i,1}^{\mathrm{out}}$	$\boldsymbol{\lambda}_{i,2}^{\mathrm{in}}$	$\boldsymbol{\lambda}_{i,2}^{\mathrm{out}}$	$\boldsymbol{\lambda}_{i,3}^{\mathrm{in}}$	$\boldsymbol{\lambda}_{i,3}^{\mathrm{out}}$
$\mathcal{BOI}$	0.2	0.22608	1	1	–	–
$\mathcal{CHP}_{1/2/3}$ (th)	0.5	0.46035	1	1	–	–
$\mathcal{CHP}_{1/2/3}$ (el)	0.1	0.20251	1	1	–	–
$\mathcal{AC}$	0.2	0.25006	0.60778	0.48792	1	1
$\mathcal{CC}$	0.2	0.31204	0.70497	0.59543	1	1
$\mathcal{HP}$	0.2	0.21584	1	1	–	–

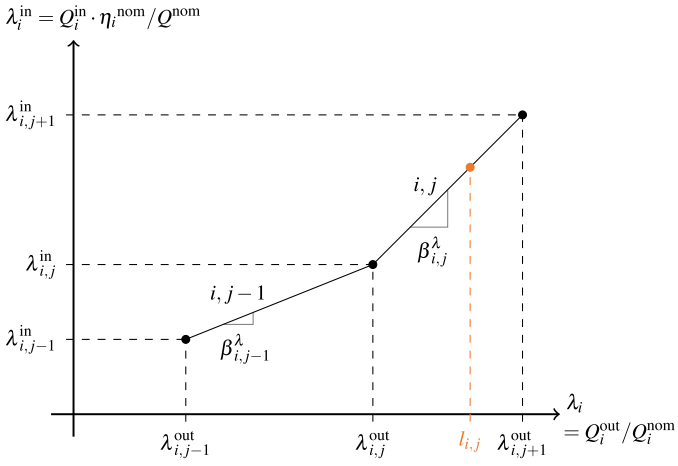

Fig. C.1. Piecewise linearization of part-load behavior of component $i \in \mathcal{U}$ adapted from Majewski et al. (2017)

rather than linearizing the nonlinear functions $\boldsymbol{\eta}_i$ for the considered components $i \in \mathcal{U}$. Note that we linearize based on normalized variables λ_i and $\lambda_i^{\mathrm{in}} := Q_i^{\mathrm{in}} \cdot \boldsymbol{\eta}^{\mathrm{nom}}/\boldsymbol{Q}_i^{\mathrm{nom}}$.

We apply a piecewise linearization as depicted in Fig. C.1.

In fact, the feasible interval of variable $\lambda_i \in [\boldsymbol{\lambda}_i^{\min}, 1]$ is decomposed into $\left|\mathcal{J}^{\lambda}\right| = n^{\lambda}$ intervals with supporting points $\boldsymbol{\lambda}_i^{\min} = \boldsymbol{\lambda}_{i,0}^{\mathrm{out}} < \ldots < \boldsymbol{\lambda}_{i,n^{\lambda}-1}^{\mathrm{out}} < \boldsymbol{\lambda}_{i,n^{\lambda}}^{\mathrm{out}} = 1, \ j = \left\{0, \ldots, n^{\lambda}\right\}$ for any component $i \in \mathcal{U}$. For each time step $t \in \mathcal{T}$, the independent variable $l_{i,j}$ in interval $j \in \mathcal{J}^{\lambda}$ is switched on or off by a binary $b_{i,j}^{\lambda} \in \{0, 1\}$

$$\boldsymbol{\lambda}_{i,j}^{\mathrm{out}} \cdot b_{i,j}^{\lambda} \leq l_{i,j} \leq \boldsymbol{\lambda}_{i,j+1}^{\mathrm{out}} \cdot b_{i,j}^{\lambda} \quad \forall\ j \in \mathcal{J}^{\lambda}\setminus\left\{n^{\lambda}\right\}, \forall\ i \in \mathcal{U} \ .$$

In this way, at most one interval can be active

$$\sum_{j\in\mathcal{J}^{\lambda}} b_{i,j}^{\lambda} \leq 1 \quad \forall\ i \in \mathcal{U}$$

and the resulting load fraction λ_i is obtained by

$$\lambda_i = \sum_{j\in\mathcal{J}^{\lambda}} l_{i,j} \quad \forall\ i \in \mathcal{U} \ .$$

Based on supporting points $\left(\boldsymbol{\lambda}_{i,j}^{\mathrm{in}}, \boldsymbol{\lambda}_{i,j}^{\mathrm{out}}\right)$, the slope parameter $\boldsymbol{\beta}_{i,j}^{\lambda}$ of the line segments j is given by

$$\boldsymbol{\beta}_{i,j}^{\lambda} = \frac{\boldsymbol{\lambda}_{i,j+1}^{\mathrm{in}} - \boldsymbol{\lambda}_{i,j}^{\mathrm{in}}}{\boldsymbol{\lambda}_{i,j+1}^{\mathrm{out}} - \boldsymbol{\lambda}_{i,j}^{\mathrm{out}}} \quad \forall\ j \in \mathcal{J}^{\lambda}, \forall\ i \in \mathcal{U} \ .$$

This yields the piecewise linear formulation

$$\lambda_i^{\mathrm{in}} = \sum_{j\in\mathcal{J}^{\lambda}} b_{i,j}^{\lambda} \cdot \boldsymbol{\lambda}_{i,j}^{\mathrm{in}} + \boldsymbol{\beta}_{i,j}^{\lambda} \cdot \left(l_{i,j} - \boldsymbol{\lambda}_{i,j}^{\mathrm{out}} \cdot b_{i,j}^{\lambda}\right) \quad \forall\ i \in \mathcal{U} \ . \tag{C.2}$$

Note that load fraction $l_{i,j}$ equals 0 if the binaries $b_{i,j}^{\lambda}$ of all intervals $\forall\ j \in \mathcal{J}^{\lambda}$ are 0. Example values for the linearization of the functions given in Table B.5 is given in Table C.1.

Inserting the definition of the load fraction λ_i^{in} into Eq. (C.2) with $l_{i,j} = Q_{i,j}^{\mathrm{out}}/\boldsymbol{Q}_i^{\mathrm{nom}}$ gives

$$Q_i^{\mathrm{in}} = \sum_{j\in\mathcal{J}^{\lambda}} \boldsymbol{\lambda}_{i,j}^{\mathrm{in}} \cdot \frac{b_{i,j}^{\lambda} \cdot \boldsymbol{Q}_i^{\mathrm{nom}}}{\boldsymbol{\eta}^{\mathrm{nom}}} + \frac{\boldsymbol{\beta}_{i,j}^{\lambda}}{\boldsymbol{\eta}^{\mathrm{nom}}} \cdot \left(Q_{i,j}^{\mathrm{out}} - \boldsymbol{\lambda}_{i,j}^{\mathrm{out}} \cdot b_{i,j}^{\lambda} \cdot \boldsymbol{Q}_i^{\mathrm{nom}}\right)$$
$$\forall\ i \in \mathcal{U} \tag{C.3}$$

and

$$\boldsymbol{\lambda}_{i,j}^{\mathrm{out}} \cdot b_{i,j}^{\lambda} \cdot \boldsymbol{Q}_i^{\mathrm{nom}} \leq Q_{i,j}^{\mathrm{out}} \leq \boldsymbol{\lambda}_{i,j+1}^{\mathrm{out}} \cdot b_{i,j}^{\lambda} \cdot \boldsymbol{Q}_i^{\mathrm{nom}}$$
$$\forall\ j \in \mathcal{J}^{\lambda}\setminus\left\{n^{\lambda}\right\}, \forall\ i \in \mathcal{U} \ . \tag{C.4}$$

Table C.2
Supporting points of investment costs

Comp.	$\mathbf{Q}^{\text{lb}}_{i,1}$ [kW]	$\mathbf{CAPEX}^{\text{lb}}_{i,1}$ [e]	$\mathbf{Q}^{\text{lb}}_{i,2}$ [kW]	$\mathbf{CAPEX}^{\text{lb}}_{i,2}$ [e]	$\mathbf{Q}^{\text{lb}}_{i,3}$ [kW]	$\mathbf{CAPEX}^{\text{lb}}_{i,3}$ [e]	$\mathbf{Q}^{\text{lb}}_{i,4}$ [kW]	$\mathbf{CAPEX}^{\text{lb}}_{i,4}$ [e]
$\mathcal{BOI}$	100	27680.7	2000	86955	–	–	–	–
$\mathcal{CHP}_1$	100	138090	1400	436869	–	–	–	–
$\mathcal{CHP}_2$	1400	436869	2300	643716	–	–	–	–
$\mathcal{CHP}_3$	2300	643716	3200	850563	–	–	–	–
$\mathcal{AC}$	100	71404	711	155917.5	2000	243252	–	–
$\mathcal{CC}$	400	89006	10000	1572302	–	–	–	–
$\mathcal{PV}$	5	32858.3	55	295651.5	550	2187492	–	–
$\mathcal{HP}$	5	5113.7	27	14999.4	83	31260.1	200	55486
$\mathcal{BAT}$	0	0	40	47323	120	118368	2000	1238006
$\mathcal{TES}^{\text{cool}}$	0	0	20	14492	1000	35264	25000	543968
$\mathcal{TES}^{\text{heat}}$	0	0	20	1929	23175	502079	115000	2086885

Due to product $b^{\lambda}_{i,j} \cdot \mathbf{Q}^{\text{nom}}_i$, Eqs. (C.3) and (C.4) give a piecewise linearization of function Eq. (C.1) only if the nominal capacity $\mathbf{Q}^{\text{nom}}_i$ is fixed. Otherwise, e.g., for design optimization, this bilinear product of a binary variable $b^{\lambda}_{i,j}$ and a continuous variable $\mathbf{Q}^{\text{nom}}_i$ can be linearized with the help of Glover's linearization (Glover, 1975). Thus, we substitute the bilinear product in Eqs. (C.3) and (C.4) with a new time-dependent variable $d_{i,j}$ and obtain

$$Q^{\text{in}}_i = \sum_{j \in \mathcal{J}^{\lambda}} \boldsymbol{\lambda}^{\text{in}}_{i,j} \cdot \frac{d_{i,j}}{\boldsymbol{\eta}^{\text{nom}}} + \frac{\boldsymbol{\beta}^{\lambda}_{i,j}}{\boldsymbol{\eta}^{\text{nom}}} \cdot \left(Q^{\text{out}}_{i,j} - \boldsymbol{\lambda}^{\text{out}}_{i,j} \cdot d_{i,j}\right) \quad \forall\, i \in \mathcal{U}\,,$$

$$\boldsymbol{\lambda}^{\text{out}}_{i,j} \cdot d_{i,j} \le Q^{\text{out}}_{i,j} \le \boldsymbol{\lambda}^{\text{out}}_{i,j+1} \cdot d_{i,j}$$

$$\forall\, j \in \mathcal{J}^{\lambda}, \forall\, i \in \mathcal{U}\,.$$

Moreover, bounds

$$\mathbf{Q}^{\text{min}}_i \le \mathbf{Q}^{\text{nom}}_i \le \mathbf{Q}^{\text{max}}_i$$

are replaced by

$$b^{\lambda}_{i,j} \cdot \mathbf{Q}^{\text{min}}_i \le d_{i,j} \le b^{\lambda}_{i,j} \cdot \mathbf{Q}^{\text{max}}_i \tag{C.5}$$

$$\left(1 - b^{\lambda}_{i,j}\right) \cdot \mathbf{Q}^{\text{min}}_i \le \mathbf{Q}^{\text{nom}}_i - d_{i,j} \le \left(1 - b^{\lambda}_{i,j}\right) \cdot \mathbf{Q}^{\text{max}}_i\,. \tag{C.6}$$

On the one hand, Eq. (C.5) guarantees that the new variable $d_{i,j}$ is 0 if the corresponding binary $b^{\lambda}_{i,j}$ equals 0. On the other hand, variable $d_{i,j}$ equals capacity $\mathbf{Q}^{\text{nom}}_i$ if binary $b^{\lambda}_{i,j}$ equals 1 due to Eq. (C.6).

C2. Linearization of investment costs

Analogously to C.1, we can replace the nonlinear investment costs

$$\mathbf{CAPEX}_i\left(\mathbf{Q}^{\text{nom}}_i\right) = \mathbf{CAPEX}^0_i \cdot \left(\frac{\mathbf{Q}^{\text{nom}}_i}{\mathbf{Q}^0_i}\right)^{\gamma_{6,i}}$$

with

$$\mathbf{CAPEX}_i\left(\mathbf{Q}^{\text{nom}}_i\right) = \sum_{j \in \mathcal{J}} b_{i,j} \cdot \mathbf{CAPEX}^{\text{lb}}_{i,j} + \quad \boldsymbol{\beta}^{Q}_{i,j} \cdot \left(\mathbf{Q}^{\text{nom}}_{i,j} - \mathbf{Q}^{\text{lb}}_{i,j} \cdot b_{i,j}\right)$$

$$\boldsymbol{\beta}^{Q}_{i,j} = \frac{\mathbf{CAPEX}^{\text{lb}}_{i,j+1} - \mathbf{CAPEX}^{\text{lb}}_{i,j}}{\mathbf{Q}^{\text{lb}}_{i,j+1} - \mathbf{Q}^{\text{lb}}_{i,j}} \qquad \forall\, j \in \mathcal{J}^{Q}$$

$$\mathbf{Q}^{\text{nom}}_i = \sum_{j \in \mathcal{J}} \mathbf{Q}^{\text{nom}}_{i,j}$$

$$\mathbf{Q}^{\text{lb}}_{i,j} \cdot b^{Q}_{i,j} \le \mathbf{Q}^{\text{nom}}_{i,j} \le \mathbf{Q}^{\text{lb}}_{i,j+1} \cdot b^{Q}_{i,j} \qquad \forall\, j \in \mathcal{J}^{Q} \backslash \{n^{Q}\}$$

$$\sum_{j \in \mathcal{J}^{Q}} b^{Q}_{i,j} \le 1$$

$$b^{Q}_{i,j} \in \{0,1\} \qquad \forall\, j \in \mathcal{J}^{Q}\,,$$

where the feasible interval of variable $\mathbf{Q}^{\text{nom}}_i \in \left[\mathbf{Q}^{\text{min}}_i, \mathbf{Q}^{\text{max}}_i\right]$ is decomposed into $\left|\mathcal{J}^{Q}\right| = n^{Q}$ intervals with bounds $\mathbf{Q}^{\text{min}}_i = \mathbf{Q}^{\text{lb}}_{i,0} < \ldots < \mathbf{Q}^{\text{lb}}_{i,n-1} < \mathbf{Q}^{\text{lb}}_{i,n^{Q}} = \mathbf{Q}^{\text{max}}_i$, $j \in \mathcal{J}^{Q}$ for any unit $i \in \mathcal{U}$. Example values of the supporting points $\left(\mathbf{CAPEX}^{\text{lb}}_{i,j}, \mathbf{Q}^{\text{lb}}_{i,j}\right)$ for the considered components are given in Table C.2.

Note that the nonlinear function $\mathbf{CAPEX}_i$ only depends on the independent variable $\mathbf{Q}^{\text{nom}}_i$ apart from constant parameter values and, thus, is either constant (operational optimization) or univariate (design optimization). In contrast to C.1, the application of Glover's linearization is therefore not necessary for the linearization of the investment costs $\mathbf{CAPEX}_i$.

Appendix D. Smoothing of efficiency regarding minimum load fraction

In this section, we include the minimum load fraction into the dynamic model equations of boiler and CHP, see Section B.3, to show the expandability of the presented model equations. More precisely, the hyperbolic tangent is used as a smooth switching function between turned off mode and an operation with a load fraction larger than the minimum load fraction. Thus, no binary controls are introduced and, in particular, we can avoid adding a combinatorial complexity to a dynamic model.

As a complication, the turned off mode with load fraction $\lambda_i = 0$ poses a stable point of the dynamics in Eq. (B.5). In fact, point $(\frac{\mathrm{d}\lambda_i}{\mathrm{dt}}, \lambda_i) = (0,0)$ cannot be escaped independent of the chosen control value Q^{in}_i

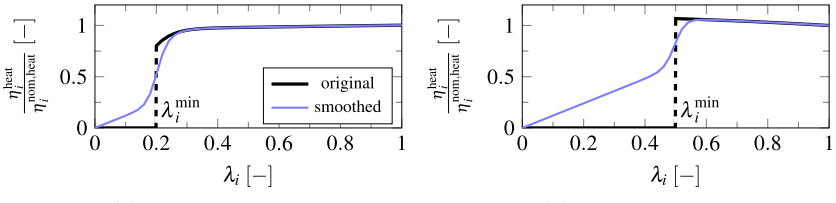

(a) Boiler, $i \in \mathcal{BOI}$ (b) CHP, $i \in \mathcal{CHP}$

Fig. D.1. Relative efficiency with minimum load fraction $\boldsymbol{\lambda}^{\text{min}}_i$, $i \in \mathcal{BOI} \cup \mathcal{CHP}$ as given in Table B.5

$$\frac{\mathrm{d}\lambda_i}{\mathrm{dt}}|_{\lambda_i=0} = \frac{1}{\boldsymbol{\tau}_i} \cdot \left(\boldsymbol{\eta}_i^{\mathrm{heat/cool}}(\lambda_i)|_{\lambda_i=0} \cdot \frac{Q_i^{\mathrm{in}}}{\boldsymbol{Q}_i^{\mathrm{nom}}} - 0 \right)$$
$$= \frac{1}{\boldsymbol{\tau}_i} \cdot \left(0 \cdot \frac{Q_i^{\mathrm{in}}}{\boldsymbol{Q}_i^{\mathrm{nom}}} - 0 \right) = 0 \qquad \forall\ i \in \mathcal{C}\ .$$

without a binary control turning the boiler or CHP explicitly on. Therefore, the zero-operation below the minimum load fraction is replaced by a linear operation with sufficient slope, see Fig. D.1. As the result, original efficiency $\boldsymbol{\eta}_i^{\mathrm{heat}}(\lambda_i),\ i \in \mathcal{BOI} \cup \mathcal{CHP}$ is replaced by the adapted smooth efficiency

$$\left(0.5 + 0.5 \cdot \tanh\left(\boldsymbol{\gamma}_1 \cdot (\lambda_i - \boldsymbol{\lambda}_i^{\min})\right)\right) \cdot \boldsymbol{\eta}_i^{\mathrm{heat}}(\lambda_i)$$
$$+ \left(0.5 - 0.5 \cdot \tanh\left(\boldsymbol{\gamma}_1 \cdot (\lambda_i - \boldsymbol{\lambda}_i^{\min})\right)\right) \cdot (\boldsymbol{\gamma}_2 + \boldsymbol{\gamma}_3 \cdot \lambda_i)\ ,$$

in Eq. (B.5). As an example, parameter values $\boldsymbol{\gamma}_1 = 30,\ \boldsymbol{\gamma}_3 = 1.2$, and $\boldsymbol{\gamma}_2 = 0.0001$ are chosen.

References

Adeodu, O., Omell, B., Chmielewski, D.J., 2019. On the theory of economic MPC: ELOC and approximate infinite horizon EMPC. J. Process Control 73, 19–32. doi:10.1016/j.jprocont.2018.09.013.

Andiappan, V., 2017. State-Of-The-Art Review of Mathematical Optimisation Approaches for Synthesis of Energy Systems. Process Integr. Optim. Sustain. 1 (3), 165–188. doi:10.1007/s41660-017-0013-2.

Appino, R.R., Ordiano, J., Mikut, R., Faulwasser, T., Hagenmeyer, V., 2018. On the use of probabilistic forecasts in scheduling of renewable energy sources coupled to storages. Appl. Energy 210, 1207–1218. doi:10.1016/j.apenergy.2017.08.133.

Augenstein, E., Herbergs, S., Kuperjans, I., Lucas, K., et al., 2005. Simulation of industrial energy supply systems with integrated cost optimization. In: 18th International Conference on Efficiency, Cost, Optimization, Simulation and Environmental Impact of Energy Systems.

Bahl, B., Lützow, J., Shu, D., Hollermann, D.E., Lampe, M., Hennen, M., Bardow, A., 2018. Rigorous synthesis of energy systems by decomposition via time-series aggregation. Comput. Chem. Eng. 112, 70–81. doi:10.1016/j.compchemeng.2018.01.023.

Bahl, B., Söhler, T., Hennen, M., Bardow, A., 2018. Typical periods for two-stage synthesis by time-series aggregation with bounded error in objective function. Front. Energy Res. 5, 35. doi:10.3389/fenrg.2017.00035.

Barton, P.I., 2009. Energy Systems Engineering. In: deBritoAlves, R.M., doNascimento, C.A., Biscaia, E.C. (Eds.), 10th International Symposium on Process Systems Engineering. In: Computer-aided chemical engineering, 27, pp. 55–57.

Barz, T., Seliger, D., Marx, K., Sommer, A., Walter, S.F., Bock, H.G., Körkel, S., 2018. State and state of charge estimation for a latent heat storage. Control Eng. Pract. 72, 151–166. doi:10.1016/j.conengprac.2017.11.006.

Baumann, H., Tillman, A.-M., 2014. The Hitch Hiker's Guide to LCA: an Orientation in Life Cycle Assessment Methodology and Application. Studentlitteratur, Lund.

Baumgärtner, N., Bahl, B., Hennen, M., Bardow, A., 2019. RiSES3: Rigorous Synthesis of Energy Supply and Storage Systems via time-series relaxation and aggregation. Comput. Chem. Eng. 127, 127–139. doi:10.1016/j.compchemeng.2019.02.006.

Baumgärtner, N., Delorme, R., Hennen, M., Bardow, A., 2019. Design of low-carbon utility systems: Exploiting time-dependent grid emissions for climate-friendly demand-side management. Appl. Energy 247, 755–765. doi:10.1016/j.apenergy.2019.04.029.

BDEW, 2019. Bundesverband der energie- und wasserwirtschaft e.v., https://www.bdew.de/energie/standardlastprofile-strom/. [accessed Jul 24, 2019].

Beykal, B., Boukouvala, F., Floudas, C.A., Pistikopoulos, E.N., 2018. Optimal design of energy systems using constrained grey-box multi-objective optimization. Comput. Chem. Eng. 116, 488–502.

Biegler, L.T., Grossmann, I.E., 2004. Retrospective on optimization. Comput. Chem. Eng. 28 (8), 1169–1192. doi:10.1016/j.compchemeng.2003.11.003.

Blanc, C., Rufer, A., 2008. Multiphysics and energetic modeling of a vanadium redox flow battery. In: 2008 IEEE International Conference on Sustainable Energy Technologies, pp. 696–701.

Braun, P., Faulwasser, T., Grüne, L., Kellett, C., Weller, S., Worthmann, K., 2018. Hierarchical distributed ADMM for predictive control with applications in power networks. IFAC J. Syst. Control 3, 10–22. doi:10.1016/j.ifacsc.2018.01.001.

Broverman, S.A., 2010. Mathematics of Investment and Credit, 5th ACTEX Publications, Inc..

Bürger, A., Zeile, C., Altmann-Dieses, A., Sager, S., Diehl, M., 2018. An algorithm for mixed-integer optimal control of solar thermal climate systems with MPC-capable runtime. In: 2018 European Control Conference (ECC), pp. 1379–1385.

Bussieck, M.R., Drud, A.S., Meeraus, A., 2003. MINLPLib - A collection of test models for mixed-integer nonlinear programming. INFORMS J. Comput. 15 (1), 114–119.

Caspari, A., Bremen, A., Faust, J., Jung, F., Kappatou, C., Sass, S., Vaupel, Y., Hannemann-Tamás, R., Mhamdi, A., Mitsos, A., 2019. Dyos - a framework for optimization of large-scale differential algebraic equation systems. In: Kiss, A.A., Zondervan, E., Lakerveld, R., Özkan, L. (Eds.), 29th European Symposium on Computer Aided Process Engineering. In: Computer Aided Chemical Engineering, 46. Elsevier, pp. 619–624. doi:10.1016/B978-0-12-818634-3.50104-1.

Coakley, D., Raftery, P., Keane, M., 2014. A review of methods to match building energy simulation models to measured data. Renew. Sustain. Energy Rev. 37, 123–141. doi:10.1016/j.rser.2014.05.007.

Constantinescu, E.M., Zavala, V.M., Rocklin, M., Lee, S., Anitescu, M., 2011. A computational framework for uncertainty quantification and stochastic optimization in unit commitment with wind power generation. IEEE Trans. Power Syst. 26 (1), 431–441. doi:10.1109/TPWRS.2010.2048133.

Dimplex, 2019. Technical data LA 60TU, http://www.dimplex.de/pdf/en/produktattribute/produkt_1726829_extern_egd.pdf. [accessed Jan 25, 2019].

Downs, J.J., Vogel, E.F., 1993. A plant-wide industrial process control problem. Comput. Chem. Eng. 17 (3), 245–255. doi:10.1016/0098-1354(93)80018-I.

DWD Climate Data Center (CDC), 2018. Historical hourly station observations from 2018, version v006, ftp://ftp-cdc.dwd.de/pub/CDC/. [accessed Jul 24, 2019].

DyOS, 2019. http://permalink.avt.rwth-aachen.de/?id=295232. [accessed Sep 17, 2019].

ENERCON, 2015. ENERCON product overview, https://www.enercon.de/fileadmin/Redakteur/Medien-Portal/broschueren/pdf/en/ENERCON_Produkt_en_06_2015.pdf. [accessed Jan 25, 2019].

Engell, S., 2007. Feedback control for optimal process operation. JPC 17, 203–219.

Engell, S., Harjunkoski, I., 2012. Optimal operation: Scheduling, advanced control and their integration. Comput. Chem. Eng. 47, 121–133. doi:10.1016/j.compchemeng.2012.06.039.

Fabrizio, E., 2008. Modelling of multi-energy systems in buildings. Politecnico di Torino and Institut National des Sciences Appliquées de Lyon.

Faulwasser, T., Engelmann, A., 2019. Toward economic NMPC for multistage ac optimal power flow. Optim. Control Appl. Method. doi:10.1002/oca.2487.

Faulwasser, T., Engelmann, A., Mühlpfordt, T., Hagenmeyer, V., 2018. Optimal power flow: an introduction to predictive, distributed and stochastic control challenges. at - Automatisierungstechnik 66 (7), 573–589. doi:10.1515/auto-2018-0040.

Federal Environment Office, 2018. Process oriented database for environmental management systems, http://www.probas.umweltbundesamt.de/php/index.php. [accessed Apr 13, 2018].

Frangopoulos, C.A., 2018. Recent developments and trends in optimization of energy systems. Energy 164, 1011–1020. doi:10.1016/j.energy.2018.08.218.

Frangopoulos, C.A., von Spakovsky, M.R., Sciubba, E., 2002. A brief review of methods for the design and synthesis optimization of energy systems. Int. J. Appl. Thermodyn. 5 (4), 151–160.

Fu, J., Faust, J.M., Chachuat, B., Mitsos, A., 2015. Local optimization of dynamic programs with guaranteed satisfaction of path constraints. Automatica 62, 184–192. doi:10.1016/j.automatica.2015.09.013.

Ghobeity, A., Mitsos, A., 2012. Optimal design and operation of a solar energy receiver and storage. ASME J. Solar Energy Eng. 134 (3), 031005:1–9.

Gill, P.E., Murray, W., Saunders, M.A., 2005. SNOPT: an SQP algorithm for large-scale constrained optimization. SIAM Rev. 47 (1), 99–131. doi:10.1137/s0036144504446096.

Glover, F., 1975. Improved linear integer programming formulations of nonlinear integer problems. Manag. Sci. 22 (4), 455–460.

Goderbauer, S., Comis, M., Willamowski, F.J.L., 2019. The synthesis problem of decentralized energy systems is strongly NP-hard. Comput. Chem. Eng. 124, 343–349. doi:10.1016/j.compchemeng.2019.02.002.

Grainger, J., Stevenson, W., 1994. Power System Analysis. McGraw-Hill Series in Electrical and Computer Engineering: Power and Energy. McGraw-Hill, New York.

Grossmann, I.E., Biegler, L.T., 2004. Part II. Future perspective on optimization. Comput. Chem. Eng. 28 (8), 1193–1218. doi:10.1016/j.compchemeng.2003.11.006.

Guillén-Gosálbez, G., 2011. A novel MILP-based objective reduction method for multi-objective optimization: Application to environmental problems. Comput. Chem. Eng. 35 (8), 1469–1477. doi:10.1016/j.compchemeng.2011.02.001.

Harb, H., Boyanov, N., Hernandez, L., Streblow, R., Müller, D., 2016. Development and validation of grey-box models for forecasting the thermal response of occupied buildings. Energy Build. 117, 199–207. doi:10.1016/j.enbuild.2016.02.021.

Harb, H., Paprott, J.-N., Matthes, P., Schütz, T., Streblow, R., Müller, D., 2015. Decentralized scheduling strategy of heating systems for balancing the residual load. Build. Environ. 86, 132–140. doi:10.1016/j.buildenv.2014.12.015.

HECI, 2019. https://www.helmholtz.de/en/research/energy/energy-system-2050/heci/. [accessed Oct 11, 2019].

Hidalgo Gonzalez, I., Kanellopoulos, K., De Felice, M., Bocin, A., 2019. JRC Open Power Plants Database (JRC-PPDB-OPEN). European Commission, Joint Research Centre (JRC) [Dataset] PID: http://data.europa.eu/89h/9810feeb-f062-49cd-8e76-8d8cfd488a05. [accessed Sep 17, 2019].

Hollermann, D. E., Goerigk, M., Hoffrogge, D. F., Hennen, M., Bardow, A., 2019. Flexible here-and-now decisions for two-stage multi-objective optimization: Method and application to energy system design selection. arXiv:1906.08621.

Hörsch, J., Hofmann, F., Schlachtberger, D., Brown, T., 2018. PyPSA-Eur: an open optimisation model of the European transmission system. Energy Strat. Rev. 22, 207–215. doi:10.1016/j.esr.2018.08.012.

Howells, M., Rogner, H., Strachan, N., Heaps, C., Huntington, H., Kypreos, S., Hughes, A., Silveira, S., Carolis, J.D., Bazillian, M., Roehrl, A., 2011. OSeMOSYS: the open source energy modeling system: an introduction to its ethos, structure and development. Energy Policy 39 (10), 5850–5870. doi:10.1016/j.enpol.2011.06.033.

Hunter, K., Sreepathi, S., Carolis, J.F.D., 2013. Modeling for insight using Tools for energy model optimization and analysis (Temoa). Energy Econ. 40, 339–349. doi:10.1016/j.eneco.2013.07.014.

IBM Corporation, 2015. IBM ILOG CPLEX Optimization Studio, Version 12.6. User Guide.
IEEE, 2018. http://sites.ieee.org/pes-testfeeders/resources/. [accessed Oct 26, 2018].
Jing, R., Wang, M., Zhang, Z., Liu, J., Liang, H., Meng, C., Shah, N., Li, N., Zhao, Y., 2019. Comparative study of posteriori decision-making methods when designing building integrated energy systems with multi-objectives. Energy Build. 194, 123–139. doi:10.1016/j.enbuild.2019.04.023.
Kadam, J., Marquardt, W., 2007. Integration of economical optimization and control for intentionally transient process operation. In: Findeisen, R., Allgöwer, F., Biegler, L. (Eds.), Assessment and Future Directions of Nonlinear Model Predictive Control. In: Lecture Notes in Control and Information Sciences, 358. Springer Berlin Heidelberg, pp. 419–434.
Koch, T., Achterberg, T., Andersen, E., Bastert, O., Berthold, T., Bixby, R. E., Danna, E., Gamrath, G., Gleixner, A. M., Heinz, S., Lodi, A., Mittelmann, H., Ralphs, T., Salvagnin, D., Steffy, D. E., Wolter, K., 2017. MIPLIB - the Mixed Integer Programming LIBrary. [accessed 02. March 2018].
Kreider, J.F., Curtiss, P., Rabl, A., 2010. Heating and Cooling of Buildings: Design for Efficiency. Mechanical Engineering Series, rev 2 ed CRC Press Taylor & Francis Group.
Lara, C.L., Mallapragada, D.S., Papageorgiou, D.J., Venkatesh, A., Grossmann, I.E., 2018. Deterministic electric power infrastructure planning: Mixed-integer programming model and nested decomposition algorithm. Eur. J. Oper. Res. 271 (3), 1037–1054. doi:10.1016/j.ejor.2018.05.039.
Li, X., Barton, P.I., 2015. Optimal design and operation of energy systems under uncertainty. J. Process Control 30, 1–9. doi:10.1016/j.jprocont.2014.11.004.
Luppi, P.A., Braccia, L., Rullo, P.G., Zumoffen, D.A.R., 2018. Plantwide Control Design Based on the Control Allocation Approach. Ind. Eng. Chem. Res. 57 (1), 268–282. doi:10.1021/acs.iecr.7b02966.
Majewski, D.E., Wirtz, M., Lampe, M., Bardow, A., 2017. Robust multi-objective optimization for sustainable design of distributed energy supply systems. Comput. Chem. Eng. 102, 26–39. doi:10.1016/j.compchemeng.2016.11.038.
Mancarella, P., 2014. MES (multi-energy systems): an overview of concepts and evaluation models. Energy 65, 1–17. doi:10.1016/j.energy.2013.10.041.
Matke, C., Bienstock, D., Munoz, G., Yang, S., Kleinhans, D., Sager, S., 2016. Robust optimization of power network operation: storage devices and the role of forecast errors in renewable energies. In: International Workshop on Complex Networks and their Applications, pp. 809–820.
Mattsson, S.E., Elmqvist, H., 1997. Modelica - An International Effort to Design the Next Generation Modeling Language. IFAC Proceed. 30 (4), 151–155. doi:10.1016/S1474-6670(17)43628-7.
Mavrotas, G., 2009. Effective implementation of the epsilon-constraint method in multiobjective mathematical programming problems. Appl. Math. Comput. 213 (2), 455–465.
McCarl, B. A., Rosenthal, R. E., 2016. McCarl GAMS User Guide, Version 24.7.
Mehleri, E.D., Sarimveis, H., Markatos, N.C., Papageorgiou, L.G., 2012. A mathematical programming approach for optimal design of distributed energy systems at the neighbourhood level. Energy 44 (1), 96–104. doi:10.1016/j.energy.2012.02.009.
Mitsos, A., Asprion, N., Floudas, C.A., Bortz, M., Baldea, M., Bonvin, D., Caspari, A., Schäfer, P., 2018. Challenges in process optimization for new feedstocks and energy sources. Comput. Chem. Eng. 113, 209–221. doi:10.1016/j.compchemeng.2018.03.013.
Mühlpfordt, T., Faulwasser, T., Hagenmeyer, V., 2018. A generalized framework for chance-constrained optimal power flow. Sustainable Energy, Grids and Networks 16, 231–242. doi:10.1016/j.segan.2018.08.002. ArXiv:1803.08299
Murray, A., Faulwasser, T., Hagenmeyer, V., 2018. Comparison of battery scheduling formulations with asymmetric charging and discharging costs. In: Proceedings of 10th IFAC Symposium on Control of Power and Energy Systems (CPES).
Obara, S., 2007. Equipment arrangement planning of a fuel cell energy network optimized for cost minimization. Renew. Energy 32 (3), 382–406. doi:10.1016/j.renene.2006.02.012.
Open Energy Modelling Initiative, 2019. http://openmodinitiative.org. [accessed Feb 19, 2019].
Park, H., Ruellan, M., Bouvet, A., Monmasson, E., Bennacer, R., 2011. Thermal parameter identification of simplified building model with electric appliance. In: 11th International Conference on Electrical Power Quality and Utilisation (EPQU), 2011. IEEE, Piscataway, NJ, pp. 1–6. doi:10.1109/EPQU.2011.6128822.
Peeters, L., Van der Veken, J., Hens, H., Helsen, L., D'haeseleer, W., 2008. Control of heating systems in residential buildings: Current practice. Energy Build. 40 (8), 1446–1455.
Perez, K.X., Baldea, M., Edgar, T.F., 2016. Integrated HVAC management and optimal scheduling of smart appliances for community peak load reduction. Energy Build. 123, 34–40. doi:10.1016/j.enbuild.2016.04.003.
Pintarič, Z.N., Kravanja, Z., 2015. The importance of proper economic criteria and process modeling for single- and multi-objective optimizations. Comput. Chem. Eng. in press. doi:10.1016/j.compchemeng.2015.02.008.
Rech, S., 2019. Smart energy systems: guidelines for modelling and optimizing a fleet of units of different configurations. Energies 12 (7), 1–36. doi:10.3390/en12071320.
Ren, H., Gao, W., Ruan, Y., 2009. Economic optimization and sensitivity analysis of photovoltaic system in residential buildings. Renew. Energy 34 (3), 883–889. doi:10.1016/j.renene.2008.06.011.
Ringkjøb, H.-K., Haugan, P.M., Solbrekke, I.M., 2018. A review of modelling tools for energy and electricity systems with large shares of variable renewables. Renew. Sustain. Energy Rev. 96, 440–459. doi:10.1016/j.rser.2018.08.002.
Roald, L., Misra, S., Krause, T., Andersson, G., 2017. Corrective control to handle forecast uncertainty: A chance constrained optimal power flow. IEEE Transactions on Power Systems 32 (2), 1626–1637. doi:10.1109/TPWRS.2016.2602805.
Sager, S., 2012. A benchmark library of mixed-integer optimal control problems. Mix. Integer Nonlinear Program. 154, 631–670.
Sakalis, G., Tzortzis, G., Frangopoulos, C., 2019. Intertemporal static and dynamic optimization of synthesis, design, and operation of integrated energy systems of ships. Energies 12, 893. doi:10.3390/en12050893.
Sass, S., Mitsos, A., 2019. Optimal operation of dynamic (energy) systems: When are quasi-steady models adequate? Comput. Chem. Eng. 124, 133–139. doi:10.1016/j.compchemeng.2019.02.011.
Schütz, T., Schraven, M.H., Remy, S., Granacher, J., Kemetmüller, D., Fuchs, M., Müller, D., 2017. Optimal design of energy conversion units for residential buildings considering German market conditions. Energy 139, 895–915. doi:10.1016/j.energy.2017.08.024.
Schütz, T., Streblow, R., Müller, D., 2015. A comparison of thermal energy storage models for building energy system optimization. Energy Build. 93, 23–31. doi:10.1016/j.enbuild.2015.02.031.
Serban, R., Petra, C., Hindmarsh, A. C., 2018. User Documentation for IDAS v2.2.1. Center for Applied Scientic Computing, Lawrence Livermore National Laboratory.
Shcherbina, O., Neumaier, A., Sam-Haroud, D., Vu, X.-H., Nguyen, T.-V., 2002. Benchmarking global optimization and constraint satisfaction codes. In: International Workshop on Global Optimization and Constraint Satisfaction. Springer, pp. 211–222.
Singer, A.B., Barton, P.I., 2006. Global optimization with nonlinear ordinary differential equations. J. Glob. Optim. 34 (2), 159–190.
Smith, R., 2005. Chemical Process: Design and Integration. John Wiley & Sons.
Srinivasan, B., Bonvin, D., 2019. 110th anniversary: a feature-based analysis of static real-time optimization schemes. Ind. Eng. Chem. Res. 58 (31), 14227–14238. doi:10.1021/acs.iecr.9b02327.
Steen, D., Stadler, M., Cardoso, G., Groissböck, M., DeForest, N., Marnay, C., 2015. Modeling of thermal storage systems in MILP distributed energy resource models. Appl. Energy 137, 782–792. doi:10.1016/j.apenergy.2014.07.036.
Tesla, 2019. Tesla Powerwall, https://www.tesla.com/sites/default/files/pdfs/powerwall/Powerwall%202_AC_Datasheet_en_northamerica.pdf. [accessed Aug 19, 2019].
Touretzky, C.R., Baldea, M., 2016. A hierarchical scheduling and control strategy for thermal energy storage systems. Energy Build. 110, 94–107. doi:10.1016/j.enbuild.2015.09.049.
University of Washington, 2018. https://www2.ee.washington.edu/research/pstca/. [accessed Oct 26, 2018].
Vanderbei, R., et al., 2004. Nonlinear optimization models, http://www.gamsworld.org/performance/princetonlib/princetonlib.htm. [accessed Sep 17, 2019].
Voll, P., 2013. Automated optimization based synthesis of distributed energy supply systems. RWTH Aachen University, Aachen.
Voll, P., Klaffke, C., Hennen, M., Bardow, A., 2013. Automated superstructure-based synthesis and optimization of distributed energy supply systems. Energy 50, 374–388.
Wilkins, A.K., Tidor, B., White, J., Barton, P.I., 2009. Sensitivity analysis for oscillating dynamical systems. SIAM J. Sci. Comput. 31 (4), 2706–2732.
Williams, T.J., Otto, R.E., 1960. A generalized chemical processing model for the investigation of computer control. Trans. Am. Inst. Electr. Eng. Part I 79 (5), 458–473. doi:10.1109/TCE.1960.6367296.
Wirth, H., Schneider, K., 2019. Aktuelle Fakten zur Photovoltaik in Deutschland. Fraunhofer ISE.
Zhang, Q., Martín, M., Grossmann, I.E., 2019. Integrated design and operation of renewables-based fuels and power production networks. Comput. Chem. Eng. 122, 80–92. doi:10.1016/j.compchemeng.2018.06.018.
Zhang, R., Nie, Y., Lam, K.P., Biegler, L.T., 2014. Dynamic optimization based integrated operation strategy design for passive cooling ventilation and active building air conditioning. Energy Build. 85, 126–135. doi:10.1016/j.enbuild.2014.09.032.
Zimmerman, A.H., 2004. Self-discharge losses in lithium-ion cells. IEEE Aerosp. Electron. Syst. Mag. 19 (2), 19–24. doi:10.1109/MAES.2004.1269687.